The Astrophysical Journal, 699:89–104, 2009 July 1 doi:10.1088/0004-637X/699/1/89

FEEDBACK FROM CENTRAL BLACK HOLES IN ELLIPTICAL GALAXIES. I. MODELS WITH EITHER RADIATIVE OR MECHANICAL FEEDBACK BUT NOT BOTH

Luca Ciotti[1], Jeremiah P. Ostriker[2,3], and Daniel Proga[4]
[1] Department of Astronomy, University of Bologna, via Ranzani 1, I-40127, Bologna, Italy
[2] Princeton University Observatory, Princeton, NJ, USA
[3] IoA, Cambridge, UK
[4] Department of Physics and Astronomy, University of Nevada, Las Vegas, NV, USA
Received 2009 January 8; accepted 2009 April 23; published 2009 June 9

ABSTRACT

The importance of the radiative feedback from massive black holes at the centers of elliptical galaxies is not in doubt, given the well-established relations among electromagnetic output, black hole mass, and galaxy optical luminosity. In addition, feedback due to mechanical and thermal deposition of energy from jets and winds emitted by the accretion disk around the central black hole is also expected to occur and has been included in the work of several investigators. In this paper, we improve and extend the accretion and feedback physics explored in our previous papers to include also a physically motivated model of mechanical feedback, in addition to radiative effects. In particular, we study the evolution of an isolated elliptical galaxy with the aid of a high-resolution one-dimensional hydrodynamical code, where the cooling and heating functions include photoionization and Compton effects, and restricting to models which include only radiative or only mechanical feedback (in the form of nuclear winds). We confirm that for Eddington ratios above 0.01 both the accretion and radiative output are forced by feedback effects to be in burst mode, so that strong intermittencies are expected at early times, while at low redshift the explored models are characterized by smooth, very sub-Eddington mass accretion rates punctuated by rare outbursts. However, the explored models always fail some observational tests. If we assume the high mechanical efficiency of $10^{-2.3}$ adopted by some investigators, we find that most of the gas is ejected from the galaxy, the resulting X-ray luminosity is far less than is typically observed and little supermassive black hole (SMBH) growth occurs. But models with low enough mechanical efficiency to accommodate satisfactory SMBH growth tend to allow too strong cooling flows and leave galaxies at $z = 0$ with E+A spectra more frequently than is observed. In a surprising conclusion, we find that both types of feedback are required. Radiative heating over the inner few kiloparsecs is needed to prevent calamitous cooling flows, and mechanical feedback from active galactic nucleus winds, which affects primarily the inner few hundred parsecs, is needed to moderate the luminosity and growth of the central SMBH. Models with combined feedback are explored in a forthcoming paper.

Key words: accretion, accretion disks – black hole physics – galaxies: active – galaxies: nuclei – galaxies: starburst – quasars: general

Online-only material: color figure

1. INTRODUCTION

All massive bulges and elliptical galaxies contain massive black holes at their center (hereafter SMBHs, e.g., see Kormendy & Richstone 1995; de Zeeuw 2001; Ferrarese & Ford 2005), and when gas is added to the central regions for any reason the SMBH will accrete and emit energy. It is also clear that SMBHs have played an important role in the processes of galaxy formation and evolution (e.g., see Silk & Rees 1998; Fabian 1999; Burkert & Silk 2001; Cavaliere & Vittorini 2002; King 2003; Wyithe & Loeb 2003; Haiman et al. 2004; Granato et al. 2004; Sazonov et al. 2005; Murray et al. 2005; Di Matteo et al. 2005; Begelman & Nath 2005; Hopkins et al. 2006; Croton et al. 2006; Sijacki et al. 2007; Pipino et al. 2009a, 2009b), as strongly supported by the remarkable correlations found between host galaxy properties and the masses of their SMBHs (e.g., see Magorrian et al. 1998; Ferrarese & Merritt 2000; Gebhardt et al. 2000; Yu & Tremaine 2002; McLure & Dunlop 2002; Graham et al. 2003; Marconi & Hunt 2003; see also Somerville 2008; Ciotti 2009).

This basic fact leads immediately to a set of interrelated questions which must be addressed before we can understand either the resultant masses of the central SMBHs or the codependency of active galactic nucleus (AGN) feedback and galactic evolution, i.e., (1) what physical processes control the SMBH accretion rate? For a given accretion rate, what form does the energy feedback take (photons, nuclear winds, and jets)? (2) How do these three forms of feedback, in turn, affect the accretion rate?

In our prior papers (Ciotti & Ostriker 1997, 2001, 2007, hereafter CO97, CO01, and CO07; Ostriker & Ciotti 2005, hereafter OC05), we have focused on the radiative, electromagnetic (EM) component, since that is most easily observed and our knowledge of it is most certain (e.g., see Sazonov et al. 2004, 2007, 2008), and we already provided indications that accretion feedback is the obvious solution to several related problems, such as the long-lasting "cooling-flow" problem, and the fate of the large amounts of gas injected into the galaxy by the passively evolving stellar populations (e.g., Peterson & Fabian 2006; see also Binney 2001). This conclusion is also supported by other investigations implementing physically motivated feedback mechanisms (e.g., see Tabor & Binney 1993; Binney & Tabor 1995; Omma et al. 2004; Churazov et al. 2005; Antonuccio-Delogu & Silk 2008), and the computed solutions are characterized by relaxation oscillations (e.g., Cowie et al. 1978; Milosavljevic et al. 2008). The general emerging picture is that energy out-

put (radiative or mechanical) from the central SMBH pushes matter out, the accretion rate drops precipitously and the expanding matter drives shocks into the galactic gas. Then the resulting hot bubble ultimately cools radiatively (it is thermally unstable) and the consequent infall leads to renewed accretion; the cycle repeats, with the galaxy being seen alternately as an AGN/starburst for a small fraction of the time and as a "normal" elliptical hosting an incipient cooling catastrophe for much longer intervals. Nowadays, several observations support the finding that accretion on central SMBHs is in fact a highly unsteady phenomenon (e.g., see Martini 2004; Goncalves et al. 2008; Prochaska & Hennawi 2009; Hopkins & Hernquist 2008).

However, although our previous work has stressed the significance of *radiative* heating near to the SMBH (in addition to the well-known Eddington momentum input, e.g., see Dorodnitsyn et al. 2008; Shi & Krolik 2008), other investigators (e.g., Binney & Tabor 1995; Tabor & Binney 1993; Begelman & Nath 2005; Begelman & Ruszkowski 2005; Di Matteo et al. 2005; Springel et al. 2005) have focused on the also important but highly uncertain *mechanical* feedback.[5] An obvious source of mechanical feedback is certainly represented by the radiatively driven winds from the broad-line regions (BLRs), whose parameters are well observed (e.g., Chartas et al. 2003, 2007; Crenshaw et al. 2003; Blustin et al. 2007; Hamann et al. 2008), so that their energy, momentum, and mass input can be added to the codes in a fairly direct way. Although the overall efficiency of such inputs appears to be modest, this component of feedback couples with great effectiveness to the ambient gas. In addition, highly collimated jets, especially at low Eddington ratios are observed to put out energy in amounts comparable to the EM output, but it is not clear how efficiently such narrow jets can couple to the ambient fluid (see Vernaleo & Reynolds 2006).

The purpose of the current paper is to introduce a *physically based* modeling of mechanical energy input to our code, and to supplement the detailed treatment of radiative effects, in a fashion that is consistent with current theory and guided by observations. At the same time, we further improve the galaxy models used for the simulations, both in the stellar and dark matter distributions, following the results of the latest observational works. In particular, in this paper we restrict our exploration to purely radiative and purely mechanical feedback, in order to better understand the specific properties of the two mechanisms when considered separately. Other aspects of purely mechanical models are investigated in detail in M.-S. Shin et al. (2009, in preparation, hereafter Paper II), while we reserve to a third paper (L. Ciotti & J. P. Ostriker 2009, in preparation, hereafter Paper III) the discussion of models in which both radiative and mechanical feedback effects are included in the hydrodynamical code. Finally, the X-ray observational properties of the most successful models will be presented in S. Pellegrini et al. (2009, in preparation, hereafter Paper IV; see also Pellegrini et al. 2009), to be compared with the results of observational works (e.g., O'Sullivan et al. 2003; Diehl & Statler 2008).

We continue to find that the situation is inherently complex. Mechanical energy output of the AGN is lower than the EM output but couples more effectively to ambient gas and thus is optimal in the innermost few hundred parsecs in shielding the SMBH from excessive accretion. But the radiation heating input to the galaxy is carried primarily by long mean free path (X-ray) photons and is most effective in heating the inner several kiloparsecs and thus moderating or forestalling cooling catastrophes in the ambient interstellar medium (ISM) of the galaxy. We tentatively conclude the BLR winds do have an essential effect in regulating SMBH accretion and, with the radiation heating feedback, cooperate in removing significant amounts of gas from giant ellipticals (see Schawinski et al. 2009) but that the jets largely escape from isolated galaxies. However, for brightest cluster galaxies, the energetic jets can provide significant input to the cluster gas—thereby helping to prevent or moderate cluster cooling-flow catastrophes (e.g., Voit & Donahue 2005; Peterson & Fabian 2006; Rafferty et al. 2008; McCarthy et al. 2008).

The paper is organized as follows. In Section 2, we describe how the new galaxy models adopted in the simulations are built, the details of the input physics (focusing in particular on the physics of accretion disk and on the mechanical feedback), and their numerical implementation. In Section 3, we present two different classes of models, both of them presenting some interesting aspects but overall failing to reproduce the situation observed in real galaxies. We thus have a first class of models in which only radiative heating is taken into account, and a second class in which only mechanical feedback is considered. Finally, in Section 4 we discuss the main results obtained.

2. THE MODELS

The galaxy models and the input physics adopted for the simulations have been improved with respect to our previous explorations. In the following we describe the new ingredients of the current models, while for the unchanged parts we refer to our previous papers: a comparative summary of the present and past treatments is given in Table 1.

2.1. Structure and Internal Dynamics

In CO97 and CO01 the galaxy models utilized a King (1972) stellar distribution plus a quasi-isothermal dark matter halo, in line with the models then used for cooling-flow studies. However, the existence of large cores of constant surface brightness has been clearly ruled out, as *Hubble Space Telescope* (*HST*) observations have shown how the central surface brightness profile is described by a power law as far in as it can be observed, i.e., to $\sim$10 pc from the center for Virgo ellipticals (e.g., see Jaffe et al. 1994; Faber et al. 1997; Lauer et al. 2005). In Pellegrini & Ciotti (1998) and in CO07 a stellar density distribution described by the more appropriate Hernquist (1990) model has been adopted, and also the dark matter halo was described by a Hernquist profile, which is quite similar in its central regions to the dark matter halos obtained from cosmological simulations (e.g., Dubinski & Carlberg 1991; Navarro et al. 1997; Fukushige & Makino 1997).

However, the Hernquist profile is characterized (as the de Vaucouleurs $R^{1/4}$ density profile) by a sizable central depression in the isotropic velocity dispersion, which is not observed. This problem is now fixed. In fact, the velocity dispersion of the Jaffe (1983) profile is monotonically decreasing. In addition, observations support the idea that ellipticals are characterized by a *total* density distribution well described by a r^{-2} profile (e.g., see Treu & Koopmans 2002, 2004; Rusin et al. 2003; Rusin & Kochanek 2005; Koopmans et al. 2006; Gavazzi et al. 2007; Czoske et al. 2008; Dye et al. 2008). For these reasons,

[5] Note that also a purely radiative feedback produces ultimately some form of mechanical feedback, in the form of shock waves, e.g., CO01 and CO07, or in the form or radiation-driven winds as found in two-dimensional and three-dimensional simulations (Proga 2007a, 2007b; Proga et al. 2008; Kurosawa & Proga 2008, 2009).

Table 1
Synoptic Table of Feedback Model Development

Input Physics	CO97	CO01	OC05	CO07	Paper I (Radiative)	Paper I (Mechanical)	Paper III
(1)	(2)	(3)	(4)	(5)	(6)	(7)	(8)
Galaxy model	King+QIH	King+QIH	King+QIH	Hernquist+Hernquist	Jaffe in SIS	Jaffe in SIS	Jaffe in SIS
Star formation	No	No	No	Yes	Yes	Yes	Yes
Circumnuclear disk	No	No	No	Yes	Yes	Yes	Yes
ADAF	No	Yes[a]	No	No	Yes	Yes	Yes
Heating and cooling							
Compton	Yes[b]	Yes[b]	Yes	Yes	Yes	Only cooling[c]	Yes
Photoionization	No	No	Yes	Yes	Yes	Only cooling[c]	Yes
Radiation pressure							
e^- scattering	Yes	Yes	Yes	Yes	Yes	No[d]	Yes
Photoionization	No	No	No	Yes	Yes	No[d]	Yes
Dust	No	No	No	Yes	Yes	No[d]	Yes
Mechanical feedback							
AGN wind	No	No	No	No[d]	No[d]	Yes	Yes
AGN jet	No	No	No	No	No[d]	No[d]	No[d]

Notes. Different names indicate the papers as in the text. Paper I indicates this paper; Paper III; QIH, quasi-isothermal halo; SIS, singular isothermal sphere: in the present models the stellar density is immersed in a dark matter halo so that the total density profile is proportional to r^{-2}.
[a] Only a few test models were computed.
[b] In CO97 a very high Compton temperature T_X for the emitted accretion luminosity spectral distribution was used, while in CO01 a large range of values for T_X was explored. Starting from OC05 the value of $T_X \simeq 2 \times 10^7$ K was fixed according to the observational estimates of Sazonov et al. (2004).
[c] Heating computed but not added to the hydrodynamics.
[d] Computed but not added to the hydrodynamics.

here we adopt Jaffe stellar models embedded in a dark halo so that the total mass profile decreases as r^{-2}. Therefore, the stellar density profile of the galaxy models is

$$\rho_* = \frac{M_* r_*}{4\pi r^2 (r_* + r)^2}, \quad (1)$$

where M_* and r_* are the total stellar mass and the scale length of the galaxy, respectively; we recall that for the Jaffe model the effective radius is $R_e = r_*/0.7447$. The total density profile is then given by

$$\rho_T = \frac{\mathcal{R} M_*}{4\pi r_* r^2}, \quad (2)$$

where the dimensionless factor $\mathcal{R} \geqslant 1$ controls the amount of dark matter contained within the half-mass radius of the stellar component. With this choice, the circular velocity of the model is given by $v_c = \sqrt{G\mathcal{R}M_*/r_*}$. The presence of significant amounts of dark matter in the central regions of normal galaxies remains controversial (e.g., see Binney & Evans 2001), but in general observational studies in the optical (e.g., Saglia et al. 1993; Bertin et al. 1994; Cappellari et al. 2006; Douglas et al. 2007) and in X-rays (e.g., Fabian et al. 1986; Humphrey et al. 2006) seems to indicate that dark matter begins to be dynamically important at 2–3R_e. For these reasons we fix $\mathcal{R}$ to the minimum admissible value $\mathcal{R} = 1$, corresponding to the same amount of dark and visible matter within the spatial half-mass radius of the stellar distribution.

All the dynamical and phase-space properties of the resulting two-component galaxy models are given in Ciotti et al. (2008), and here we report only the formulae for the quantities of interest: in particular, the model central projected velocity dispersion $\sigma_\circ$ (obtained by solving and projecting the Jeans equations under the assumption of orbital isotropy) is given by

$$\sigma_\circ = \frac{v_c}{\sqrt{2}}. \quad (3)$$

Note that we do not consider the effect of M_{BH} on $\sigma_\circ$, in accordance with estimated values for the radius of the SMBH sphere of influence (e.g., Riciputi et al. 2005). The parameters describing the galaxy model are determined following CO07, i.e., first we assign a value for the central velocity dispersion $\sigma_\circ$, and we determine the galaxy *present-day* blue luminosity L_B and effective radius R_e from the Faber–Jackson and the fundamental plane relations (Equations (3)–(4) in CO07). We then fix the relative amount of dark matter to stars within R_e by assigning $\mathcal{R}$, thus determining the total stellar mass M_* of the galaxy and finally the stellar mass-to-light ratio $\Upsilon_* \equiv M_*/L_B$.

An important ingredient in the energetics of the gas flows, namely, the thermalization of the stellar mass losses due to the stellar velocity dispersion (e.g., see Parriott & Bregman 2008), depends on the radial trend of this latter quantity which, for the isotropic models here considered is given by

$$\rho_* \sigma_*^2 = \rho_* \sigma_{*\circ}^2 + \frac{G M_* M_{BH}}{4\pi r_*^4} \left[\frac{1 - 2s + 6s^2 + 12s^3}{3s^3(1+s)} - 4 \ln\left(1 + \frac{1}{s}\right) \right], \quad s \equiv \frac{r}{r_*}, \quad (4)$$

where $\sigma_{*\circ}$ is the isotropic one-dimensional stellar velocity dispersion without the contribution of the SMBH (Ciotti et al. 2008). Note that, at variance with the estimate of $\sigma_\circ$, in the thermalization of the stellar mass losses we also consider the (time increasing) contribution of the gravitational field of the central SMBH.

2.2. The Circumnuclear Disk and the SMBH Accretion Luminosity

At the onset of the cooling catastrophe a large amount of gas suddenly flows onto the central regions of the galaxy, and this induces star formation and accretion on the central SMBH, producing a burst of energy from the galaxy center. However, observations of our own galactic center and high-resolution

studies of other nearby systems indicate that, in addition to the central starburst with radius ∼100–300 pc, accretion onto the central SMBH is mediated by a small central gaseous disk within which additional significant star formation occurs, and the remaining fraction of gas either is blown out in a BLR wind, or it is accreted onto the central SMBH. In our treatment the disk is not simulated with hydrodynamical equations, but its description is needed to obtain important quantities required by the code. In an improvement over CO07, we now also model and add to the hydrodynamics the mechanical feedback produced by the disk wind (see Table 1), but for future reference, in the following we also describe the modeling of a nuclear jet. However, while the jet contribution to the circumnuclear disk mass balance is considered in the numerical integration, the associated mechanical feedback is not added to the current hydrodynamical simulations.

The circumnuclear disk, which is the repository of the gas inflowing at a rate $\dot{M}_1^{\rm eff}$ from the first active mesh point R_1 of the hydrodynamical grid, and which feeds the central SMBH at a rate $\dot{M}_{\rm BH}$, contains at any time the mass gas $M_{\rm dg}$ and a total stellar mass $M_{\rm d*} = M_{\rm dl*} + M_{\rm dh*}$, which is divided among low- and high-mass stars (with the division mass at 8 $M_\odot$). The disk also contains a mass $M_{\rm rem}$ of remnants from the earlier generations of evolved stars.

In the adopted scheme the accretion rate on the central SMBH is given by

$$\dot{M}_{\rm BH} = \frac{\dot{M}_{\rm fid}}{1+\eta_{\rm d}}, \tag{5}$$

where

$$\dot{M}_{t\rm fid} \equiv \frac{M_{\rm dg}}{\tau_{\rm d}}, \qquad \eta_{\rm d} \equiv \frac{\dot{M}_{\rm fid}}{2\dot{M}_{\rm Edd}}, \qquad \dot{M}_{\rm Edd} \equiv \frac{L_{\rm Edd}}{\epsilon_0 c^2} \tag{6}$$

are the fiducial depletion rate of gas from the circumnuclear disk, its normalized value, and the Eddington mass accretion rate, respectively. The reference radiative efficiency ϵ_0 is defined in Equation (8). Equations (5) and (6) are designed to guarantee that when $\eta_{\rm d} \ll 1$ the gas is accreted onto the central SMBH at the rate $\dot{M}_{\rm fid}$, while $\dot{M}_{\rm BH} = 2\dot{M}_{\rm Edd}$ for $\eta_{\rm d} \gg 1$ (i.e., we allow for possible moderate super-Eddington accretion; note however that outside the first grid point R_1 the flow accretion rate is limited in a self-consistent way by feedback effects). From Equation (5) we calculate the instantaneous bolometric accretion luminosity as

$$L_{\rm BH} = \epsilon_{\rm EM}\, \dot{M}_{\rm BH}\, c^2, \tag{7}$$

and, at variance with CO07 (see also Table 1), here we adopt an "advection-dominated accretion flow (ADAF)-like" radiative efficiency

$$\epsilon_{\rm EM} = \epsilon_0 \frac{A\dot{m}}{1+A\dot{m}}, \qquad \dot{m} \equiv \frac{\dot{M}_{\rm BH}}{\dot{M}_{\rm Edd}}, \tag{8}$$

where A is a free parameter so that $\epsilon_{\rm EM} \sim \epsilon_0 A\dot{m}$ for $\dot{m} \ll A^{-1}$. In our simulations, we fix $A = 100$ (see, e.g., Narayan & Yi 1994; CO01, where a very preliminary investigation of ADAF effects on radiative feedback was carried out), and we adopt $\epsilon_0 = 0.1$ or 0.2 (e.g., see Noble et al. 2009). As usual in accretion theory, we finally introduce the normalized accretion luminosity

$$l \equiv \frac{L_{\rm BH}}{L_{\rm Edd}} = \frac{A\dot{m}^2}{1+A\dot{m}}, \tag{9}$$

where the last expression derives from the ADAF phenomenological description.

There are a few *lag times* in our problem which are expressed as follows. The first is the *instantaneous disk lag time*, appearing in Equation (6), and already considered in CO07, defined as

$$\tau_{\rm d} \equiv \frac{2\pi}{\alpha}\sqrt{\frac{R_{\rm d}^3}{GM_{\rm BH}}}, \tag{10}$$

where $\alpha \simeq 10^{-2} - 10^{-1}$ is the disk viscosity coefficient and $R_{\rm d}$ and $M_{\rm BH}$ are the instantaneous values of the fiducial radius of the circumnuclear disk and the mass of the central SMBH. In CO07, the disk radius $R_{\rm d}$ was maintained fixed to R_1, instead now we use the scaling predicted by thin-disk theory

$$R_{\rm d}(t) = f_d R_1 \times \left(\frac{M_{\rm BH}}{M_{\rm BH0}}\right)^{2/3} \tag{11}$$

(e.g., see Morgan et al. 2007) where $M_{\rm BH0}$ is the central SMBH mass at the beginning of the simulation. We assume $f_d = 0.4$, so that $R_{\rm d}(0) \simeq 2$ pc for an initial SMBH mass of $\simeq 10^8\, M_\odot$.

The second characteristic time (that was not considered in CO07) is the instantaneous *infall* lag time from R_1 to the disk, estimated as

$$\tau_{\rm i} = \frac{R_1}{v_{\rm ff}}, \qquad v_{\rm ff} \equiv \sqrt{\frac{2GM_{\rm BH}}{R_1}}, \tag{12}$$

so that the effective rate at which gas accretes on the disk is obtained by solving the differential equation

$$\frac{d\dot{M}_1^{\rm eff}}{dt} = \frac{\dot{M}_1 - \dot{M}_1^{\rm eff}}{\tau_{\rm i}}, \tag{13}$$

where $\dot{M}_1$ is the instantaneous rate at which gas flows through the first active grid point.[6] It follows that when $\dot{M}_1$ provided by hydrodynamics drops to zero the circumnuclear disk experiences a fueling declining exponentially with time.

The disk total gas mass $M_{\rm dg}$ is not only the source of SMBH accretion, but also of star formation in the disk: we assume that a fraction of $M_{\rm dg}$ is converted into stars at a rate $\eta_*\dot{M}_{\rm fid}$ (where $\eta_* \simeq 10 M_{\rm dg}/M_{\rm BH}$), and that another fraction of $M_{\rm dg}$ is lost as a *disk wind* and as a *jet* at instantaneous rates given by $\eta_{\rm w}\dot{M}_{\rm BH}$ and $\eta_{\rm j}\dot{M}_{\rm BH}$, so that the equation for the gas mass in the disk is

$$\frac{dM_{\rm dg}}{dt} = \dot{M}_1^{\rm eff} - (1+\eta_{\rm w}+\eta_{\rm j})\dot{M}_{\rm BH} - \eta_*\dot{M}_{\rm fid}. \tag{14}$$

Note that the presence of a jet was not considered in CO07, so that $\eta_{\rm j} = 0$ therein. The stars formed in the disk are described separately as a function of their mass, i.e., high-mass stars ($M > M_{\rm II} = 8\, M_\odot$) produce a total disk mass $M_{\rm dh*}$, and low-mass stars ($M_{\rm inf} < M < M_{\rm II}$) contribute to a disk mass $M_{\rm dl*}$ according to the equations

$$\frac{dM_{\rm dl*}}{dt} = (1-f_{\rm h})\eta_*\dot{M}_{\rm fid} - \frac{M_{\rm dl*}}{\tau_{*\rm l}}; \qquad \frac{dM_{\rm dh*}}{dt} = f_{\rm h}\eta_*\dot{M}_{\rm fid} - \frac{M_{\rm dh*}}{\tau_{*\rm h}}. \tag{15}$$

For the characteristic evolutionary times we adopt $\tau_{*\rm l} = \tau_{\rm opt}$ and $\tau_{*\rm h} = \tau_{\rm II}$ given in CO07, while we assume $f_{\rm h} = 0.5$, corresponding to a top-heavy Salpeter-like initial mass function

[6] $\dot{M}_1$ is taken positive in case of accretion and zero in case of outflow at R_1.

(e.g., see Nayakshin & Sunyaev 2005, Nayakshin et al. 2006) of slope $x \simeq 1.16$ and minimum mass $M_{\rm inf} = 0.1\,M_\odot$. The associated optical ($L_{\rm d,opt}$) and UV ($L_{\rm d,UV}$) luminosities of the stellar disk are calculated following the scheme described in CO07. Finally, stellar remnants mass in the disk evolves as

$$\frac{dM_{\rm rem}}{dt} = f_{\rm rem,l}\frac{M_{\rm dl*}}{\tau_{*\rm l}} + f_{\rm rem,h}\frac{M_{\rm dh*}}{\tau_{*\rm h}}, \quad (16)$$

where $f_{\rm rem,l} = 0.2$, $f_{\rm rem,h} = 0.09$.

The equation for the mass loss associated with the disk wind is

$$\frac{dM_{\rm dw}}{dt} = \eta_{\rm w}\dot{M}_{\rm BH} + (1 - f_{\rm rem,l})\frac{M_{\rm dl*}}{\tau_{*\rm l}} + (1 - f_{\rm rem,h})\frac{M_{\rm dh*}}{\tau_{*\rm h}}, \quad (17)$$

the first term is a mass loss driven as a wind by the central SMBH, and the second and third are from high-mass and low-mass stars in the central disk.

At variance with CO07, where the effects of mechanical feedback were not considered and the wind treatment was extremely simplified, here we explore two different classes of models, that we call *Type A* and *Type B*. In particular, we use for the ratio of the wind outflow rate to the SMBH accretion rate

$$\eta_{\rm w} \equiv \begin{cases} 2, & \text{[A]} \\ \dfrac{3\eta_{\rm w}^{\rm M}}{4}\dfrac{l}{1+0.25l}, & \text{[B].} \end{cases} \quad (18)$$

Therefore, Type A models correspond to the models in CO07. In case of Type B models, whose parameterization is introduced to mimic the results of two-dimensional simulations, the efficiency of ejecting a wind increases with increasing Eddington ratio, $\eta_{\rm w}^{\rm M}$ fixes the maximum value of $\eta_{\rm w}$, and the factor 3/4 takes into account the maximum possible value for the scaled accretion luminosity l. The situation is illustrated in the bottom panel of Figure 1, where the solid lines represent the coefficient $\eta_{\rm w}$ for Type A models (black) and Type B models (red, with $\eta_{\rm w}^{\rm M} = 1800\epsilon_{\rm w}^{\rm M}$). As a consequence of this choice, winds in Type A models eject more mass at low accretion luminosities, while the opposite happens in Type B models for $l \gtrsim 1/3$.

In particular, our scaling of the radiation-driven wind mass-loss rate and mechanical power is motivated both by current simulations and by observations of massive outflows from quasars (e.g., Ganguly & Brotherton 2008; Holt et al. 2008). Some quasars show broad absorption lines (BALs) which are the most dramatic evidence for winds in AGN. BALs are almost always blueshifted relative to the emission-line rest frame, indicating the presence of outflows from the active nucleus, with velocities as large as $0.2c$ (e.g., Turnshek 1988). BALs are observed not only in the UV but also in the X-rays: for example, Chartas et al. (2003) discovered a very BAL in the X-ray spectrum of PG 1115+80. It is commonly accepted that these mass outflows in quasars are very likely disk winds driven by radiation from accretion disks (e.g., see Königl 2006; Proga 2007a).

Of course, determining the mass-loss rate and mechanical power based on observations requires modeling, because observations do not directly provide the information about the wind column density and photoionization structure (e.g., Arav et al. 2007, and references therein). In addition, one must assume something about the wind covering factor. Therefore, a physical model of disk winds is needed to complement data analysis and to estimate the key wind properties. In particular, hydrodynamical simulation of radiation-driven disk winds allows us to explore the impact upon the mass-loss rate, $\dot{M}_{\rm dw}$ and outflow geometry caused by varying the system luminosity and the radiation field geometry. For example, Proga et al. (1998) showed that winds driven from, and illuminated solely by, an accretion disk yield *complex, unsteady outflow*. In this case, time-independent quantities can be determined only after averaging over several flow timescales. On the other hand, if winds are illuminated by radiation mainly from the central engine, then the disk yields steady outflow. Proga et al. (1998; see also Proga 1999) found that $\dot{M}_{\rm dw}$ is a strong function of the total luminosity, while the outflow geometry is determined by the geometry of the radiation field. In particular, for a relatively small l, there is no wind but only a puffed up disk. Then as l increases a strong equatorial wind develops. For very high l, the wind becomes bipolar. For high system luminosities $\dot{M}_{\rm dw}$ of the disk scales with the luminosity in a way similar to stellar mass-loss rate, i.e., $\dot{M}_{\rm dw} \propto l^{1.7}$ (see Castor et al. 1975). As the system luminosity drops below a critical value [$\sim 2L_{\rm Edd}/(1 + M_{\rm max})$], $\dot{M}_{\rm dw}$ decreases quickly to zero ($M_{\rm max}$ is the total line opacity for an optically thin case).

The wind power and geometry depend on the luminosity and also on the mass of SMBH. Proga & Kallman (2002, 2004; see also Proga et al. 2000) showed that for $M_{\rm BH} = 10^8\,M_\odot$ and $l \simeq 0.5$ a strong wind develops whereas for $l \simeq 0.1$ there is no disk wind (Equation (18)) for Type B models reflects this

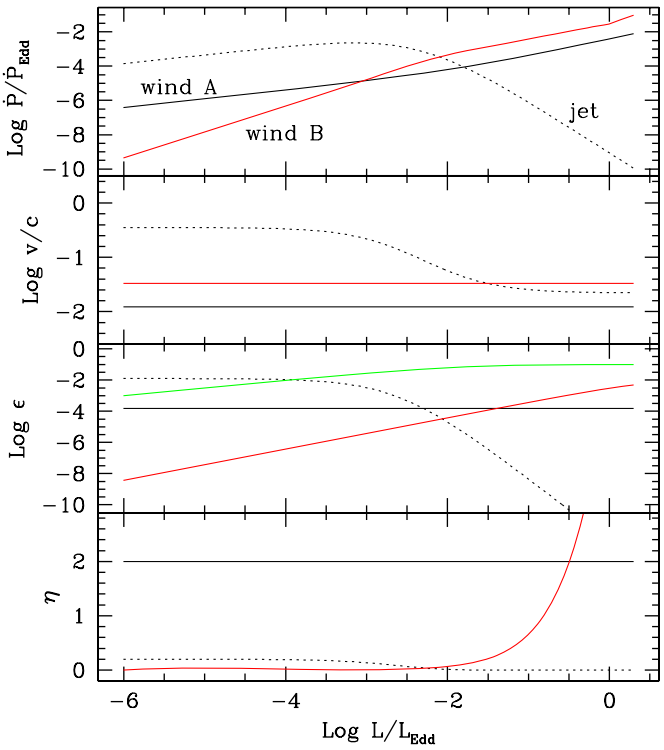

Figure 1. Mechanical feedback properties as a function of Eddington ratio l with ADAF coefficient $A = 100$ (Equation (9)). The red solid lines refer to wind properties of Type B models with maximum wind efficiency $\epsilon_{\rm w}^{\rm M} = 5 \times 10^{-3}$ and $\eta_{\rm w}^{\rm M} = 1800\epsilon_{\rm w}^{\rm M}$ (Equation (23)). From bottom to top panels: ejected mass fraction (Equations (18)–(23)); wind mechanical efficiency (Equation (21)); wind velocity (Equation (22)); normalized wind momentum per unit solid angle $\dot{P}/\dot{P}_{\rm Edd} = \sqrt{2\epsilon_{\rm w}\eta_{\rm w}}\dot{m}/(2\Delta\Omega_{\rm w})$ (where $\dot{P}_{\rm Edd} = \dot{M}_{\rm Edd}c$, see Equation (26)). The wind opening angle is given in Equation (31). The black solid lines refer to wind properties of Type A models, where $\epsilon_{\rm w} = 1.5 \times 10^{-4}$, $\eta_{\rm w} = 2$, $\Delta\Omega_{\rm w} = \pi$. The dotted lines represent the corresponding jet properties, parameterized as in Equations (19) and (24)–(26), with $\Delta\Omega_{\rm w} = 2.5 \times 10^{-2}$. Finally, the green line is the ADAF modulated EM efficiency as given by Equation (8), with $\epsilon_0 = 0.1$ and $A = 100$.

(A color version of this figure is available in the online journal.)

Table 2
Properties of Computed Models

Model	$\epsilon^{\rm M}_{\rm w}$	$\langle\epsilon_{\rm w}\rangle$	$\langle\epsilon_{\rm j}\rangle^{\rm a}$	$\langle\epsilon_{\rm EM}\rangle^{\rm a}$	$\log \Delta M_{\rm BH}$	$\log \Delta M_{*}$	$\log \Delta M_{\rm w}$	$\log M_{\rm gas}$	$\log L^{\rm eff}_{\rm BH,opt}/L_{\rm Edd}$	$\log L_{\rm X,ISM}$	$\langle\Delta\Omega_{\rm w}\rangle$	$f_{\rm duty}$
(1)	(2)	(3)	(4)	(5)	(6)	(7)	(8)	(9)	(10)	(11)	(12)	(13)
CF[b]	...	...	...	...	10.34	9.51	9.96	9.66	...	41.31	...	...
RB0$_{02}$	5×10^{-3}[a]	1.7×10^{-4}[a]	1.5×10^{-3}	0.124	9.16	10.22	10.25	9.73	−5.08	40.38	0.094	0.6 0.7
RB0	5×10^{-3}[a]	1.8×10^{-4}[a]	2.4×10^{-3}	0.057	9.45	10.36	10.29	9.69	−5.72	40.08	0.098	0.38 8.2×10^{-3}
MA0	5×10^{-3}	5×10^{-3}	1.2×10^{-2}	2.7×10^{-3}	7.17	6.43	10.38	7.65	−7.71	36.64	–	0.79 0.79
MA1	2.5×10^{-4}	2.5×10^{-4}	7.6×10^{-3}	0.038	7.56	9.21	10.41	7.99	−7.55	37.60	0.50	0.79 0.73
MA2	10^{-4}	10^{-4}	6.0×10^{-3}	0.051	7.75	9.46	10.30	9.75	−7.52	40.32	0.50	3.9×10^{-4} 0.72
MA3	5×10^{-5}	5×10^{-5}	3.7×10^{-3}	0.069	8.10	9.72	10.26	9.88	−7.55	40.76	0.50	10^{-3} 1.7×10^{-4}
MA4	3×10^{-5}	3×10^{-5}	2.0×10^{-3}	0.073	8.55	9.83	10.50	8.04	−7.76	37.81	0.50	2×10^{-3} 1.7×10^{-3}
MB0	5×10^{-3}	8.8×10^{-4}	2.2×10^{-3}	0.049	8.98	9.63	10.24	9.50	−5.88	39.91	0.46	0.92 1.1×10^{-3}
MB1	2.5×10^{-3}	5.4×10^{-4}	2.2×10^{-3}	0.053	9.11	9.68	10.28	9.27	−6.06	39.52	0.46	0.96 1.1×10^{-3}
MB2	10^{-3}	2.3×10^{-4}	2.4×10^{-3}	0.056	9.22	9.67	10.29	9.42	−6.04	39.72	0.45	3.7×10^{-2} 1.3×10^{-3}
MB3	3×10^{-4}	7.8×10^{-5}	2.2×10^{-3}	0.059	9.33	9.62	10.30	9.29	−5.92	39.49	0.43	3.9×10^{-2} 1.9×10^{-3}
MB4	10^{-4}	2.4×10^{-5}	2.3×10^{-3}	0.060	9.44	9.66	10.30	9.38	−5.46	39.41	0.43	3.9×10^{-2} 2×10^{-3}

Notes. Masses are in units of solar masses and luminosities in erg s^{-1}. In models of Class A the wind efficiency is maintained constant, i.e., $\epsilon_{\rm w}=\epsilon^{\rm M}_{\rm w}$. In models of Class B the value of $\epsilon^{\rm M}_{\rm w}$ is reached when $L_{\rm BH}=2\,L_{\rm Edd}$. In models with the subscript 02 the maximum radiative efficiency in Equation (8) is set to $\epsilon_0=0.2$ instead of 0.1 as in the other models. Mean efficiencies are calculated according to Equation (34). ΔM_* is the total amount of star formed during the model evolution, $\Delta M_{\rm w}$ is the total amount of ISM lost at 10 $R_{\rm e}$ and $M_{\rm gas}$ the instantaneous amount of gas inside 10 $R_{\rm e}$. $L^{\rm eff}_{\rm BH,opt}$ is the fiducial SMBH luminosity in the optical as would be seen at infinity after absorption, with $L^{\rm eff}_{\rm BH,opt}=0.1\,L_{\rm BH}$ at the first grid point (see CO07 for details). The luminosity-weighted wind solid opening angle $\langle\Delta\Omega_{\rm w}\rangle$ (in units of 4π) is calculated according to Equation (34), and the reported value refers to the final time of each simulation; in model MA0 the value is not reported as $L_{\rm BH}<0.1$ $L_{\rm Edd}$ over all the evolution. The duty cycle is calculated for the effective optical accretion luminosity as would be seen from infinity. The first number correspond to a universe age of 4 Gyr, the second to 13.7 Gyr, and the time span used for the computation is $\Delta t=t/2$.
[a] Figures corresponding to quantities calculated but not added to the hydrodynamical equations.
[b] The cooling-flow model CF was stopped at 8 Gyr.

trend). The primary reason for this luminosity sensitivity is the fact that the mass flux density of the wind decreases strongly with decreasing disk luminosity and the wind is more subject to overionization. Proga & Kallman (2004) also found that for a fixed Eddington fraction (e.g., 50%), it is easier to produce a wind for $M_{\rm BH}>10^7\,M_\odot$ than for $M_{\rm BH}<10^7\,M_\odot$. This result is a consequence of the decrease of the UV contribution to the disk total radiation with decreasing mass of the BH in the Shakura & Sunyaev (1973) disk model for a fixed Eddington fraction.

In addition to the treatment of CO07, we now consider another mass component ejected by disk, i.e., a *nuclear jet* with instantaneous mass flow

$$\frac{dM_{\rm j}}{dt}=\eta_{\rm j}\dot{M}_{\rm BH},\qquad \eta_{\rm j}=\frac{0.2}{(1+100l)^4}, \tag{19}$$

the trend of $\eta_{\rm j}$ as a function of l is shown in the bottom panel of Figure 1 with the dotted line: it is apparent how the mass ejected by the jet is always negligible with respect to the wind mass loss in Type A models, while it is slightly dominant over the wind in Type B models at low-luminosity ratios.

We stress that, even though we consider this additional mass component in the circumnuclear wind mass balance (Equation (14)), the associated feedback effects on the galaxy ISM are not taken into account in the simulations (see Table 1), and for the moment we are assuming that the mass, momentum, and energy fluxes in the jet escape the galaxy. In the code, all the equations presented in this section are integrated numerically with a first-order finite difference scheme.

2.3. The Mechanical Feedback Treatment

We now discuss how the kinetic energy, momentum, and mass of the BLR wind are transferred to the ISM. For sake of completeness, we also describe the jet treatment.

As in CO07, the fiducial *instantaneous mechanical luminosity* of the disk wind is given by

$$L_{\rm dw}=\epsilon_{\rm w}\dot{M}_{\rm BH}c^2+\epsilon_{\rm II}c^2(1-f_{\rm rem,h})\frac{M_{\rm dh*}}{\tau_{*\rm h}}, \tag{20}$$

where $\epsilon_{\rm w}$ is the mechanical efficiency of the wind, and the second term describes the energetic associated with the Type II supernova (SNII) explosions of the high-mass stars in the circumnuclear disk. In analogy with Equation (18), we assume

$$\epsilon_{\rm w}\equiv\begin{cases}\epsilon^{\rm M}_{\rm w}, & \text{[A]}\\ \dfrac{3\epsilon^{\rm M}_{\rm w}}{4}\dfrac{l}{1+0.25l}, & \text{[B].}\end{cases} \tag{21}$$

In Type A models we explore the range $3\times10^{-5}\leqslant\epsilon^{\rm M}_{\rm w}\leqslant5\times10^{-3}$ (see Table 2), i.e., also values significantly lower than adopted by Hernquist and collaborators (5×10^{-3}, see Di Matteo et al. 2005). For reference, in CO07 (where $\epsilon_{\rm w}$ was also kept constant), we adopted $\epsilon^{\rm M}_{\rm w}=5\,10^{-4}$, but the resulting mass, energy, and momentum sources were not added to the code. In case of Type B models, where the wind efficiency is a function of the normalized accretion luminosity, $\epsilon^{\rm M}_{\rm w}$ is the maximum possible value (reached for $l=2$), and the different values adopted in the simulations are listed in Table 2. In both cases, the *instantaneous disk wind velocity* is given by

$$v_{\rm w}\equiv\sqrt{\frac{2L_{\rm dw}}{\dot{M}_{\rm dw}}}\simeq\sqrt{\frac{2\epsilon_{\rm w}}{\eta_{\rm w}}}c, \tag{22}$$

where the last expression neglects the mass return contribution of massive stars in the circumnuclear disk (see Equation (20)). Note that in Type A models $v_{\rm w}$ is in the range $2\times10^3-2\times10^4$ km s^{-1} (as a function of the specific assumed value for

ϵ_w), in agreement with observations of BLRs (e.g., Crenshaw et al. 2003). For the same reasons, in Type B models we require $v_w = 10^4$ km s^{-1}, so that η_w^M and ϵ_w^M are linked by the relation

$$\eta_w^M = 1800\epsilon_w^M. \quad (23)$$

In analogy with the wind component, the *instantaneous jet mechanical luminosity* is written as

$$L_j = \epsilon_j \dot{M}_{BH} c^2, \qquad \epsilon_j = \frac{0.0125}{(1+400l)^4}, \quad (24)$$

and the jet velocity is given by

$$v_j \equiv \sqrt{\frac{2L_j}{\dot{M}_j}} = \sqrt{\frac{2\epsilon_j}{\eta_j}}\, c, \quad (25)$$

which, for our chosen parameterization, gives high but subrelativistic jet velocity of $v_j/c \simeq 10^{-1.65}$ for $l \gtrsim 0.1$ (see Figure 1). Note that from Equations (21) and (24) jets are far more efficient than nuclear winds at low Eddington ratios (Ghisellini 2008; Jolley & Kuncic 2008). The dependence of wind and jet velocities on the normalized accretion luminosity is shown in Figure 1 (second panel from the top), where the solid lines refer to the wind and the dotted line to the jet. Finally, the wind and jet momentum are defined as

$$m_j \equiv \dot{M}_j v_j, \qquad m_w \equiv \dot{M}_{dw} v_w. \quad (26)$$

We now illustrate how we distribute the mechanical feedback over the galaxy ISM. In the following we describe the procedure both for the wind and for the jet, even though in the hydrodynamical equations we take into account only the wind component. First, we introduce the *instantaneous wind and jet lag times*

$$\tau_{wj} \equiv \frac{R_1}{v_{wj}} \quad (27)$$

from the center to the first active grid point R_1 (where the subscript indicates the specific component—disk wind or nuclear jet—considered), and at each time step we compute the time-lagged values for mass, momentum, and kinetic energy at R_1 by solving the differential equation

$$\frac{dX_l}{dt} = \frac{X - X_l}{\tau_{wj}}, \quad (28)$$

where X_l is the generic-lagged variable associated with the instantaneous unlagged value X. Outside R_1 we then distribute mass, momentum, and kinetic energy over the hydrodynamical grid (outside R_1), by integrating numerically the phenomenological differential equation

$$\frac{\partial \ln Y_{wj}}{\partial \ln r} = -\frac{P_{ISM}(r)}{P_{wj}(r)} - \frac{r}{v_{wj}}\frac{\partial \ln Y_{wj}}{\partial t}, \quad (29)$$

where Y_{wj} is the mass, momentum, and energy of the disk wind/jet component at distance r from the center, $P_{wj}(r)$ is the local wind/jet pressure, and for each quantity $Y(R_1) = X_l$. In this paper, we restrict to simulations where the time derivative is neglected, while in Paper III also this latter term is considered. In practice, we first integrate Equation (29) for the wind/jet pressure, i.e.,

$$P_{wj} = \frac{Y_{wj}}{2\Delta\Omega_{wj} r^2}, \quad (30)$$

where Y_{wj} is the effective wind/jet momentum crossing the shell of radius r, so that Equation (29) is a nonlinear differential equation for Y_{wj}. Once the equation is integrated, the radial behavior of P_{wj} and the right-hand side of Equation (29) are known over the whole grid, and the equation can be integrated for mass and energy. We thus determine how much of the mechanical energy, momentum, and returned mass are deposited in the ISM at each radius.

A physical justification of Equation (29) is given in the Appendix, but it can be thought of phenomenologically in the following way. If the pressure corresponding to the momentum flow within the jet or wind is much greater than the pressure in the ambient gas, very little mass, momentum, and kinetic energy is taken from it and deposited in that ambient gas. But when the right-hand side of Equation (29) approaches unity, the "working surface" has been reached and the jet or wind discharges its content.

The solid angle in the denominator of Equation (30) is the opening angle of the wind and of the jet, and the factor of 2 accounts for the biconical nature of the flow. While for the jet we assumed in all the simulations the fiducial value $\Delta\Omega_j = 2.5 \times 10^{-2}$, for the wind case we adopt

$$\Delta\Omega_w = \begin{cases} \pi & \text{[A]} \\ \pi \min(\sqrt{l^2 + a^2}, 1), & \text{[B]}, \end{cases} \quad (31)$$

where case B is designed to mimic the behavior found in radiation-driven winds: higher luminosity corresponds to a larger opening angles. The constant inside the square root is fixed to $a = \Delta\Omega_j/\pi$, so that for small values of accretion luminosity the wind opening angle coincides with the jet opening angle. Finally, note that the almost linear dependence of $\Delta\Omega_w$ on l for $l > a$ assumes that the *linear* opening angle depends on $\sqrt{l}$ for this regime. The wind/jet momentum (with the opening solid angle factor) as a function of l is shown in Figure 1 (top panel), and it is apparent that this quantity is dominated by the wind contribution (solid lines) for $l \gtrsim 10^{-2}$.

To implement numerically the mechanical feedback terms, we finally compute the nuclear wind mass, momentum, and kinetic energy per unit volume deposited in each shell as

$$\text{Source}_{wj} = \frac{3}{4\pi}\frac{Y_{wj}(R_i) - Y_{wj}(R_{i+1})}{R_{i+1}^3 - R_i^3}, \quad (32)$$

and we add them (only for the wind component) to the right-hand side of Equations (56)–(58) in CO07. In practice, we assume that the quantities of mass, momentum, and kinetic energy transferred to the ISM within the opening angle are finally distributed over the whole solid angle, a forced choice for our one-dimensional code.

Summarizing, our simple formulae for Type B models capture some of the key wind properties of quasar winds: the wind opening angle, mass-loss rate, and power increase with the accretion luminosity, and the fact that there are negligible radiation pressure-driven winds for $l \lesssim 0.01$. Figure 1 shows (going downward from the top) our modeling of the inputs of momentum, velocity, energy, and mass, respectively. The simplest case of constant wind mechanical efficiency (Type A) is shown as a solid black line, whereas the one in better accord with radiatively driven winds (Type B) is shown in red. A hypothetical relativistic jet model ("radio mode") is given by the dotted lines and the green line indicates the ADAF-like treatment of the radiative efficiency. For Eddington ratios above 0.01, the

solution represents the typically observed (and computed) "AGN mode" of high radiative efficiency and low mechanical energy output efficiency, whereas at low Eddington ratios ($l \lesssim 10^{-1.5}$), the output shifts to radio mode of low EM output and high mechanical energy efficiency in a relativistic jet. As we will see most of the SMBH growth occurs in the AGN mode and so the net (mass weighted) efficiencies are in agreement with well-known estimates (e.g., Soltan 1982; Yu & Tremaine 2002; Merloni & Heinz 2008; Martinez-Sansigre & Taylor 2009), but much of the energy output occurs in the radio mode with important consequences for the energy balance in clusters of galaxies (e.g., see McNamara & Nulsen 2007, and references therein).

2.4. The Unchanged Input Physics

The stellar mass-loss rate and the Type Ia supernova (SNIa) rate associated with the initial stellar distribution are the main ingredients driving evolution of the models. In the code, the stellar mass losses—the source of *fuel* for the activity of the SMBH—follow the detailed prescriptions of the stellar evolution theory, and we use exactly the same prescriptions as in CO07 (see Sections 2.2 and 2.3 therein).

The radiative heating and cooling produced by the accretion luminosity are numerically computed as in CO07 by using the Sazonov et al. (2005) formulae, which describe the net heating/cooling rate per unit volume $\dot{E}$ of a cosmic plasma in photoionization equilibrium with a radiation field characterized by the average quasar spectral energy distribution derived by Sazonov et al. (2004; see also Sazonov et al. 2007, 2008), whose associated spectral temperature is $T_X \simeq 2$ keV. In particular, Compton heating and cooling, bremsstrahlung losses, line, and continuum heating and cooling are taken into account. Also the star formation over the galaxy body, and the radiation pressure due to electron scattering, to photoionization, and finally to UV, optical and infrared photons on dust are treated as in CO07, where the derivation and the numerical integration scheme of the radiative transport equations are described in detail. Finally, all the relevant information about the numerical code and the hydrodynamical equations can be found in CO01 and CO07.

3. MODEL EVOLUTION

We now show the main properties of representative models characterized by a stellar mass $M_* = 2.9 \times 10^{11}\, M_\odot$, a blue optical luminosity $L_B = 5\times10^{10}\, L_{B\odot}$ (corresponding to a stellar mass-to-light ratio in the blue band of $\simeq$5.8), a fundamental plane effective radius $R_e = 6.9$ kpc, and a central aperture velocity dispersion $\sigma_\circ = 260$ km s^{-1}. The stellar distribution is immersed in a dark matter halo so that the total mass density distribution is proportional to r^{-2}, and an identical amount of stellar and dark matter is contained within the stellar half-mass radius. The initial SMBH mass follows the present-day Magorrian relation, with $M_{BH} \simeq 10^{-3} M_*$, as it is believed that the bulk of the SMBH mass is assembled during the process of galaxy formation (e.g., Haiman et al. 2004; Sazonov et al. 2005), but this process is not modeled in the present simulations. Therefore, these models are not appropriate as initial conditions for cosmological simulations, because their parameters are fixed to reproduce early-type galaxies similar to those observed in the local universe (at $z = 0$), and also because we set outflow boundary conditions at the galaxy outskirts ($\sim$250 kpc): from this point of view, the simulations represent an isolated elliptical galaxy (consistently we are not considering the effects of possible merging on the galaxy evolution). A central cluster galaxy would have more difficulty generating winds and would suffer from bursts of cluster gas inflow. We adopted this framework to adhere to the standard approach followed in "cooling-flow" simulations. In future explorations, we will address in a more consistent way the problem of the galaxy structural and dynamical modifications due to star formation and mass redistribution over a Hubble time, and the compatibility of the obtained galaxies with the present-day scaling laws of elliptical galaxies. We also stress that the models presented are just a representative sample out of several tens of runs that have been made, characterized by different choices of the input parameters (often outside the currently accepted ranges).

The initial conditions for the ISM are represented by a very low density gas at the local thermalization temperature. The establishment of such high-temperature gas phase at early cosmological times is believed to be due to a "phase transition" when, as a consequence of star formation, the gas-to-stars mass ratio was of the order of 10% and the combined effect of SNIa explosions and AGN feedback became effective in heating the gas and driving galactic winds (e.g., Sazonov et al. 2005). Several theoretical arguments and much empirical evidence, such as galaxy evolutionary models and the metal content of the intracluster medium support this scenario (e.g., Renzini et al. 1993; OC05; Di Matteo et al. 2005). For the reasons above, in the simulations here presented (as well as in all others simulations not shown), we assume that the galaxy stellar component at the beginning of the simulation is 2 Gyr old, and the simulations span 12 Gyr, so that the cosmic time at the end of the simulations is 14 Gyr.

Important quantities associated with the model evolution are the mass (luminosity) accretion-weighted EM and mechanical efficiencies, defined in natural way as

$$\langle\epsilon_{EM}\rangle \equiv \frac{\int \epsilon_{EM}\dot{M}_{BH}dt}{\Delta M_{BH}}, \qquad \langle\epsilon_w\rangle \equiv \frac{\int \epsilon_w\dot{M}_{BH}dt}{\Delta M_{BH}}, \tag{33}$$

where ΔM_{BH} is the SMBH accreted mass over the time interval considered. In case of Type B models, we also compute the luminosity-weighted average fraction of the sphere covered by the wind, defined as

$$\langle\Delta\Omega_w\rangle \equiv \frac{\int 2\Delta\Omega_w L_{BH}dt}{4\pi\int L_{BH}dt}. \tag{34}$$

At variance with Equation (33), we restrict the computation of the integrals to high-luminosity phases only that we fiducially assume defined by $L_{BH} > 0.1 L_{Edd}$. Following CO07, we finally compute for the various luminosities the *duty cycle* over a period of time Δt

$$f_{duty} \equiv \frac{\left(\int_{t-\Delta t}^{t} L dt\right)^2}{\Delta t\int_{t-\Delta t}^{t} L^2 dt}; \tag{35}$$

with this definition a square wave with fraction of time f in the high state would have $f_{duty} = f$.

We summarize the properties of the models in Table 2. For reference, we first list the cooling-flow "CF" model: with no SMBH feedback (but allowance for SN feedback of types Ia and II, and taking into account the SMBH gravitational field), it allows the central SMBH to grow to mass far greater than observed in any system: clearly, AGN feedback is needed.

3.1. Purely Radiative Models

We now discuss a couple of *purely radiative* models (Table 2, models RB0 and RB0_{02}), i.e., models in which the mechanical

feedback effects are computed (following the Type B description) but not added to the hydrodynamical equations, and whose maximum radiative efficiency is $\epsilon_0 = 0.2$ ($RB0_{02}$) or $\epsilon_0 = 0.1$ (RB0), values which bracket current observational estimates for the likely bolometric radiative efficiency (e.g., Figure 2 in Yu & Tremaine 2002). We begin by noticing that we do not expect that these models will be as satisfactory as the models presented in CO07, at least for what concerns the final SMBH mass. In fact, we see from the first line in Table 1 that not only the dark matter halo is much more important at large radii than in our previous works (so that global degassing is more difficult), but also that in the central regions of the galaxy the gas is more tightly bound. This is because the stellar density profile is now proportional to r^{-2}, so that the gravitational field is stronger in the central regions; in addition, the mass return from evolving stars is correspondingly more concentrated and the radiative losses more important. Finally, radiative feedback is reduced at low accretion luminosities, due to the ADAF prescription. This reduction has significant effects: in fact, it is during the low-luminosity phases that the stellar mass losses buildup the galactic gaseous atmosphere responsible for the successive cooling catastrophe episodes. A very low accretion luminosity during the quiescent phases contributes less to the global energetic balance, the subsonic outflow at large radii (mainly due to SNIa heating) is less favored, and the time interval between the catastrophes is reduced (see also Figure 8 in CO01).

A first important result of the new models is that overall the main properties of the CO01 and CO07 models are confirmed, and episodic outbursts reaching $l \simeq 0.1$ are common. After a first evolutionary phase in which a galactic wind is sustained by the combined heating of SNIa and thermalization of stellar velocity dispersion, the central "cooling catastrophe" of the galaxy gaseous halo commences, with the formation of a collapsing cold shell at $\sim$1 kpc from the center. In the absence of the feedback from the central SMBH a "mini-inflow" would then be established, with the flow stagnation radius (i.e., the radius at which the flow velocity is zero) of the order of a few hundred parsecs to a few kiloparsecs: these decoupled flows are a specific feature of cuspy galaxy models with moderate SNIa heating (Pellegrini & Ciotti 1998). After the cooling catastrophe, the radiative feedback caused radiation pressure and radiative heating strongly affects the subsequent evolution, as can be seen in Figure 2 where we show the luminosity evolution of the central AGN with time sampling of 10^5 yr. The bolometric luminosity (top panel) ranges between 0.001 and 0.1 of the Eddington limit (the almost horizontal solid line) at peaks in the SMBH output but, since obscuration is often significant, the optical accretion luminosity as seen from infinity can be much lower (bottom panel): we note that obscuration is commonly considered the explanation for red quasars (e.g., see Wang 2008). However, the central quasar is not always obscured and we see, in the lower panels of Figure 2, that the optical luminosity exceeds $\sim 10^{44}$ erg s^{-1} in numerous bursts. As already found in CO07, the major AGN outbursts are separated by increasing intervals of time (set by the cooling time and by the secular decrease of the mass return rate from the evolving stellar population), and present a characteristic temporal substructure, whose origin is due to the cooperating effect of direct and reflected shock waves (from the inner rim of the spherical strongly perturbed zone): these outflowing shocks would be a likely place to produce emission of synchrotron radiation and electron and ionic cosmic rays, which are considered an additional source of feedback

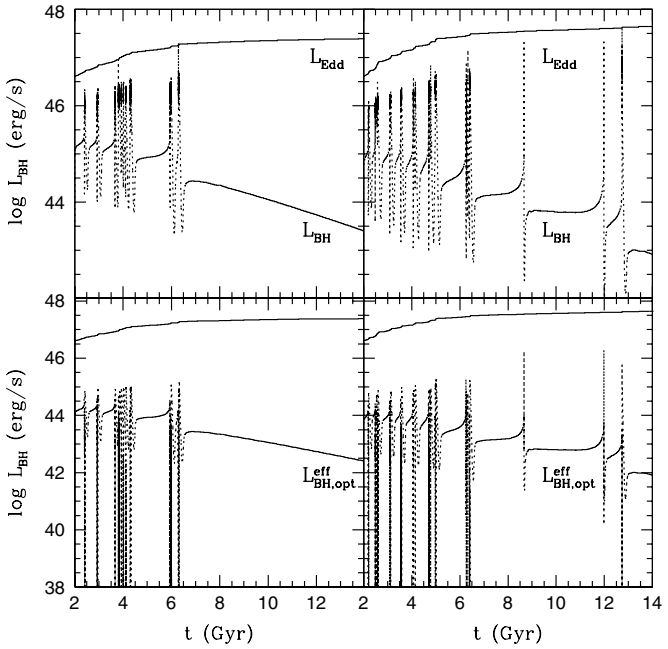

Figure 2. Purely radiative models. The dotted lines are the bolometric accretion luminosity (top) and the optical SMBH luminosity corrected for absorption, i.e., as it would be observed from infinity (bottom), for the models $RB0_{02}$(left panels), and RB0 (right panels). Model RB0 is identical to model $RB0_{02}$, but with $\epsilon_0 = 0.1$ instead of 0.2. As in CO07 at the center we fixed $L^{\rm eff}_{\rm BH,opt}(R_1) = 0.1 L_{\rm BH}$. In model $RB0_{02}$quasar-like bursts at early times are followed at late times by a very quiet and passive accretion at late times with quite low optical luminosity. With a lower radiative efficiency gas is ejected less efficiently from the galaxy and intermittent bursts persist to late times. While both models are far better than models without radiative feedback in addressing the problems caused by standard cooling flows, neither acceptably match the known properties of AGNs/young stars in massive galaxies (see Table 2).

(Jiang et al. 2009, hereafter Paper V; see also Sijacki et al. 2008).

In model $RB0_{02}$(left panels), at $t \simeq 6$ Gyr the SNIa heating, also sustained by a last strong AGN burst, becomes dominant and after a last major burst a global galactic wind takes place and the nuclear accretion switches to the optically thin regime. The SMBH mass accretion rate strongly oscillates as a consequence of radiative feedback, with peaks of the order of 10 or (more) $M_\odot$ yr^{-1}, while during the final, hot-accretion phase the almost stationary accretion is $\lesssim 10^{-2}\, M_\odot$ yr^{-1}, much less than the instantaneous mass return rate from the passively evolving stellar populations ($\dot{M}_* \lesssim 1\, M_\odot$ yr^{-1}). In the optical, $\log(L^{\rm eff}_{\rm BH,opt}/L_{\rm Edd}) \sim -5$ (see Table 2), consistent with observations (e.g., see Ho 2008). However, the absolute accretion luminosity emitted ($\sim 3 \times 10^{43}$ erg s^{-1}) is still very large when compared with some of the low-luminosity AGN observed (e.g., Pellegrini 2005a, 2005b), showing that some additional form of feedback is still needed in the low-luminosity phase of the models. Note that in the last 6 Gyr the SMBH virtually stops its growth, while the ISM mass first increases due to the high-mass return rate of the evolving stellar population, and then decreases due to the global galactic wind induced by SNIa. During the entire model evolution, a mass $\gtrsim 3 \times 10^{10}\, M_\odot$ of recycled gas has been added to the ISM from stellar mass losses. Approximately, $2.1 \times 10^{10}\, M_\odot$ has been expelled as a galactic wind, while $\sim 1.4 \times 10^{10}\, M_\odot$ has been transformed into new stars, so that only 0.7% of the recycled gas has been accreted onto the central SMBH. We note that several observational indications exist supporting the idea that, while the majority of the

stellar mass in elliptical galaxies may have formed at high redshifts, small but detectable star-formation events (summing up to $\lesssim$5%–10% of the total stellar mass) may have occurred at low redshift (e.g., see Watabe et al. 2008; Pipino et al. 2009a, 2009b; Helmboldt et al. 2008; Trager et al. 2008). Since the flow becomes nearly steady, the duty cycle approaches unity for RB02, but for RB0 the short time in a strong burst at late epoch produces a small duty cycle as observed in low redshift central SMBHs. Overall, the global behavior of these purely radiative models is very similar to the models in CO07, where we refer for details about the different evolutionary phases. Integrated values of their global quantities at the end of the simulation are listed in Table 2. Finally, it is important to stress that an identical model without SMBH feedback (i.e., $\epsilon_0 = 0$ in Equation (33)), but with the same star-formation treatment of the model just described, produced an SMBH of (the much too high) final mass $\gtrsim 10^{10}\,M_\odot$, while the total mass in new stars was reduced to $\sim 3 \times 10^9\,M_\odot$ (see model CF in Table 2). In addition, model CF does not present fluctuations in the starburst and ISM X-ray luminosities, thus showing the vital importance of SMBH feedback in the overall results.

Of course, reducing the value of the radiative efficiency from 0.2 to 0.1, the number of bursts and the final mass of the SMBH increases. In particular, note how major bursts persist to late times (right panels in Figure 2): this behavior reduces considerably the derived value of $f_{\rm duty}$ calculated at late times, and the various quantities of the model are reported in Table 2.

Are these purely radiative models an adequate representation of observed AGN/elliptical galaxies? While far better than cooling-flow models such as CF, which do not allow for radiative heating and radiation pressure caused by the AGN, they are clearly inadequate in several respects. At the end of the simulations, the ratio of the SMBH to stellar mass (also considering the added mass in new stars) is $\sim 9 \times 10^{-3}$ (for model RB0) and $\sim 4.7 \times 10^{-3}$ (for model RB0$_{02}$), larger than the canonical ratio of 0.0013 (e.g., Yu & Tremaine 2002), i.e., radiative heating alone does not suffice to limit SMBH growth to the observationally allowed degree. The luminosity from young stars is $\sim 10^{40.2}$ erg s^{-1} even at relatively low states between bursts, which would produce central regions which are far too blue compared with typical ellipticals and the AGN during these low states, while at only $10^{-4} L_{\rm Edd}$, is far more luminous (at $\sim 10^{10.2} L_\odot$) than observed AGN in their low states (see, e.g., Pellegrini 2005a, 2005b; Wrobel et al. 2008; Gallo et al. 2008; Ho 2008). Of course, from Table 2 it is apparent that a model with a peak radiative efficiency of $\epsilon_0 = 0.1$ is worst.

Are these defects due to too low an assumed radiative efficiency? For example, note that in model RB0 with a peak efficiency of 0.1, the average (i.e., weighted over the mass accretion rate, see Equation (33)) EM efficiency of this model is seen to be 0.057 which is below that found by Yu & Tremaine (2002) by applying the Soltan (1982) argument. However, model RB0$_{02}$(with a peak radiative efficiency of 0.2) has an average radiative efficiency of 0.124, but is still inadequate in representing real galaxies, especially at redshift zero. In particular, the relatively high values of the ratio $L^{\rm eff}_{\rm BH,opt}/L_{\rm Edd}$ combined with the final high values of $M_{\rm BH}$ produces central optical luminosities $\gtrsim 10^{43}$ erg s^{-1}, considerably above what is observed from nearby elliptical in the "off" state. For these reasons, we believe that the defects of the purely radiative models cannot be "fixed" by simply increasing ϵ_0; radiative feedback alone is insufficient (for massive galaxies) in limiting cooling-flow-induced star formation and central SMBH mass growth.

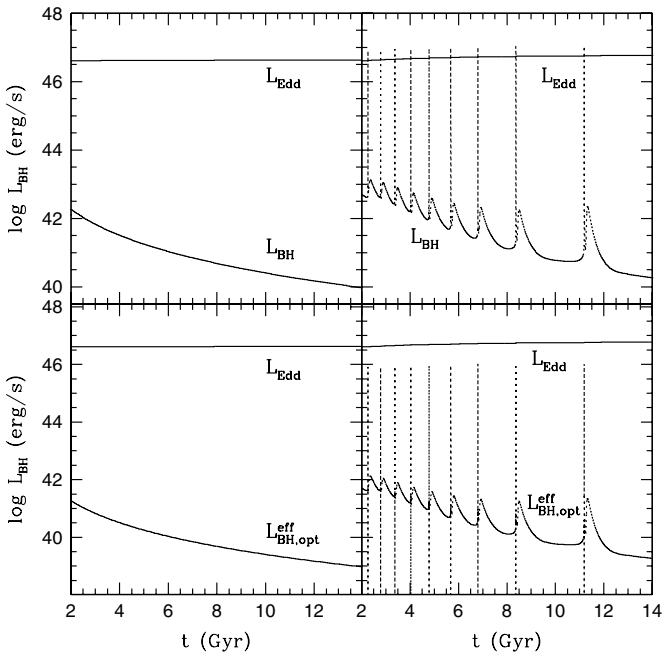

Figure 3. Purely mechanical Type A models, i.e., models with a constant nuclear wind mechanical feedback efficiency. Luminosity evolution of models MA0 ($\epsilon^{\rm M}_{\rm w} = 5 \times 10^{-3}$, left panels) and MA3 ($\epsilon^{\rm M}_{\rm w} = 5 \times 10^{-5}$, right panels). The dotted lines are the bolometric accretion luminosity (top) and the optical SMBH luminosity corrected for absorption, i.e., as it would be observed from infinity (bottom). The global properties of Type A models are given in Table 2.

3.2. Purely Mechanical Models

From the previous discussion, it follows that mechanical energy input is also required. In order to study the effects of mechanical feedback we now switch off radiation feedback (while radiative cooling is obviously maintained active), and we explore *purely mechanical* models. In some sense, these models are complementary to models RB0 and RB0$_{02}$. In a first assay, we add mechanical feedback in the simple fashion normally adopted in several investigations, as a fixed numerical efficiency for the input of mechanical energy and for the amount of gas carried out by the wind. These purely mechanical Type A models are referred in Table 2 as MA. We then present the purely mechanical models of Type B (MB models in Table 2), i.e., models in which the wind efficiency from the circumnuclear regions depends on the accretion luminosity, declining with declining values of l, as is expected for radiatively driven winds. In both families, the model identification number in Table 2 increases at decreasing wind efficiency. In this paper, we describe the general properties of the purely mechanical models, while in Paper II we focus on more specific quantitative aspects of purely mechanical Type B models.

3.2.1. Type A Models: Constant Mechanical Efficiency

In these models the constant wind mechanical efficiency ranges from $\epsilon^{\rm M}_{\rm w} = 5 \times 10^{-3}$ in model MA0, as utilized for example by Di Matteo et al. (2005) and Johansson et al. (2008), down to $\epsilon^{\rm M}_{\rm w} = 3 \times 10^{-5}$ in model MA4. The resulting global properties of the whole family are reported in Table 2.

Model MA0 (Figure 3, left panels), with the highest assumed steady efficiency is found in a state of permanent, global

wind. The fact that the accretion luminosity is very low during the entire evolution is revealed by the very low averaged value of $\langle \epsilon_{\rm EM} \rangle \simeq 2.7 \times 10^{-3}$ obtained from Equation (33), a consequence of the ADAF implementation. With the assumed high mechanical efficiency we find that (consistent with other investigators) almost all the recycled gas produced by stellar evolution is ejected from the galaxy, and a very negligible amount of mass is added to the central SMBH. In addition, also star formation is maintained at very low levels. The final X-ray thermal luminosity of the model is far too low, orders of magnitude below that seen from normal giant elliptical galaxies (e.g., O'Sullivan et al. 2003).

As we reduce $\epsilon_{\rm w}^{\rm M}$ (models MA1 and MA2), the evolution becomes more interesting. In fact, gas accumulates via the usual thermal instability, falls to the center and there generates an enormous explosion and, in a single burst, the galaxy is essentially evacuated of gas. There are no further bursts and the system is in permanent wind state until $z = 0$. This is essentially what is found by Di Matteo et al. (2005) with the only difference being that the gigantic outburst in their case is fueled by a gas-rich merger while in our case it is fed by recycled gas deposited at the center via the classic Field thermal instability. Since all of these models (MA0, MA1, and MA2) have no bursts at late times and are "on" at a nearly constant but low level, the corresponding duty cycles at late times are near unity; again, these models are too faint as thermal X-ray sources.

In model MA3 (Figure 3, right panels), the mechanical feedback is quite weak, and the galaxy presents a series of bursts, well separated by an increasing amount of time. The final SMBH mass is almost doubled, and also the new stellar mass is now significant, summing up to several $10^9\ M_\odot$. The situation is even more extreme in model MA4. These models match observations in one respect. In fact, the occurrence of numerous bursts at late times is revealed by small duty cycles (10^{-3}–10^{-4}) so that they would be seen as AGN at late times with approximately that probability, and this is roughly consistent with observations. An inspection of Table 2 also reveals that AGN feedback can be important not only to suppress star formation when cooperating with SNIa to remove the gas from the galaxy, but also to induce star formation, especially in the central regions of the galaxies. This finding was already obtained in CO07, and proposed as a possible way, in alternative or in addition to galaxy merging (e.g., Hopkins et al. 2009a, 2009b), to produce the central "extra light" observed in some elliptical galaxy (see Lauer et al. 2005).

Clearly, these models cannot represent the cosmological evolution of galaxies, as all galaxies would be found systematically at very low values of their ISM X-ray luminosity, just consistent with discrete sources, but in net disagreement with observations if considering high efficiency models. In addition, a reduction of the fixed mechanical efficiency leads to a quite strong transition to the situation in which a significant amount of mass is added to the central SMBH. In other words, purely mechanical models with constant wind efficiency appear to be quite "stiff" in their behavior, switching from a strong global wind to a recurrent and significant bursting activity when reducing the efficiency. Extreme "fine tuning" would be required to produce an acceptable model and that result would probably not be robust to the normal statistical variations of parameters describing ellipticals in the fundamental plane. Due to the computational time required, such statistical investigation is however not attempted here, and it is postponed to Paper II.

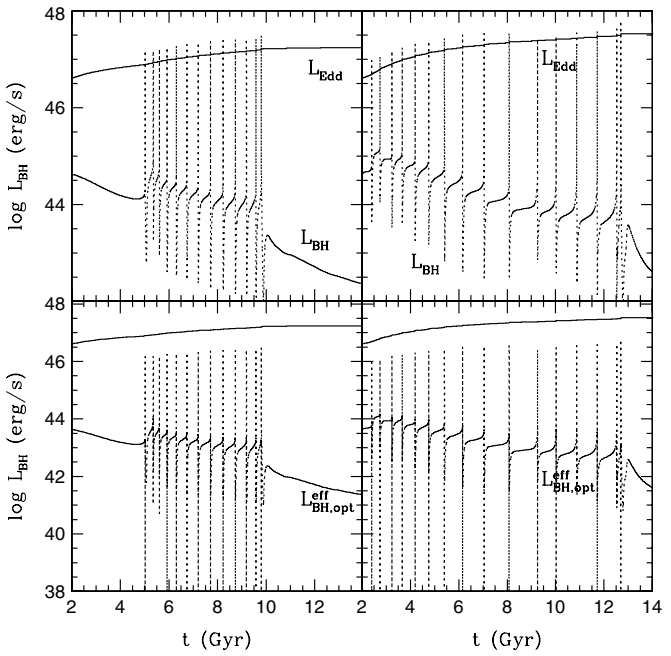

Figure 4. Purely mechanical Type B models, i.e., models with a wind mechanical efficiency dependent on the (normalized) accretion luminosity *l*. Luminosity evolution of models MB0 (the purely mechanical model associated with model RB0, left panels) and MB3 (right panels). The nuclear wind mechanical feedback efficiencies at peak are $\epsilon_{\rm w}^{\rm M} = 5 \times 10^{-3}$ and $\epsilon_{\rm w}^{\rm M} = 3 \times 10^{-4}$, respectively. The dotted lines are the bolometric accretion luminosity (top) and the optical SMBH luminosity corrected for absorption, i.e., as it would be observed from infinity (bottom). The global properties of Type B models are given in Table 2.

Guided by these results, we reduce the importance of feedback by considering a more plausible variation of the purely mechanical models (Type B models), in which the mechanical efficiency is a function of accretion luminosity, so that during bursts $\epsilon_{\rm w}$ is moderate, and drops to very low values in the low-luminosity phases between bursts, in better accord with theoretical models for radiative accretion of AGN winds.

3.2.2. Type B Models: Luminosity-Dependent Mechanical Efficiency

We now move to describe the results for the family of MB models. As in the case of MA models, the value of the (peak) mechanical efficiency decreases from model MB0 to model MB4. In particular, the peak values $\epsilon_{\rm w}^{\rm M}$ are coincident with the constant values of $\epsilon_{\rm w}$ for the pairs MA0-MB0 and MA2-MB4, so that in these models the effects of the luminosity-dependent mechanical feedback efficiency can be studied by direct comparison.

In general, the effect of the luminosity dependence of $\epsilon_{\rm w}$ in Type B models is an increase in the final mass added to the central SMBH, as can be seen from Table 2. For example, at the end of the simulations $\Delta M_{\rm BH} \sim 10^{7.17}\ M_\odot$ in model MA0, while $\Delta M_{\rm BH} = 10^{8.98}\ M_\odot$ in model MB0. Similarly, this is $\sim 10^{7.75}\ M_\odot$ in model MA2 and $10^{9.44}\ M_\odot$ in model MB4. Note that these differences are mainly produced during the low-luminosity phases, as at the peaks the mechanical efficiency is identical to the corresponding MA models, and the comparison of the luminosity evolution in the right panels of Figures 3 and 4 illustrates this difference.

As an additional example, in the right panels of Figure 4 one can see a large number of bursts during all the evolution of model MB3 ($\epsilon_{\rm w}^{\rm M} = 3 \times 10^{-4}$), while model MA1 ($\epsilon_{\rm w}^{\rm M} = 2.5 \times 10^{-4}$)

just presents a single burst. And the accreted mass of the central SMBH ($\Delta M_{\rm BH}$) is in far better agreement with observations (e.g., MB2, MB3) than it is in the models with constant accretion efficiency. The present-day luminosity ratios of the (optical) accretion luminosity to the Eddington luminosity are much smaller than in the purely radiative models, but higher than in Type A models. The duty cycles (Table 2, Column 13) are in general quite small, due to the recurrent bursting activity which is still present in the models at late epochs. It is interesting that the duration of a single burst is of the order of 10^6 yr, in accordance with observational estimates based on proximity effect (e.g., Kirkman & Tytler 2008); we also note how the luminosity-averaged EM efficiencies, both in Type A and Type B models, are in the range $0.04 \lesssim \langle\epsilon_{\rm EM}\rangle \lesssim 0.08$, in nice agreement with observational studies.

The amount of new stars formed is of the same order as in Type A models, while the final mass of the ISM (and its X-ray luminosity) is larger, due to the less efficient feedback during the low-luminosity phases. Also, the final SMBH masses are larger than those that are observed, and larger than in Type A models. Therefore, while in Type A models almost no mass is added to the central SMBH after the process of galaxy formation (and so no cosmological evolution in the $M_{\rm BH}$–σ relation is expected in the absence of merging), in Type B models a mass comparable to the initial SMBH mass is added on a cosmological time, and a consequent evolution of the $M_{\rm BH}$–σ relation is expected. We note that observations are now becoming able to probe such evolution (e.g., see Woo et al. 2008). Finally, during the low-luminosity phases, the nuclear emission is larger than what is observed in (very) low-luminosity AGNs, and this is due to the reduced contribution of the luminosity-dependent mechanical wind efficiency in Type B models.

We then conclude that an additional form of feedback is needed both during the high-luminosity phases (and this feedback is in the form of radiation, explored in Paper III, which is devoted to the study of combined models), and during the quiescent low-luminosity phases at late times. Obviously, this second form of feedback cannot be provided by radiation pressure and radiative heating as in the peak phases, and it is presumably provided by jets and/or thermally driven nuclear winds, not included in the present models. In sum, Type B models (ADAF-like) are more satisfactory than the normally computed (fixed efficiency) Type A models, but are still observationally inadequate.

4. DISCUSSION AND CONCLUSIONS

In this paper, we have investigated, with the aid of one-dimensional hydrodynamical simulations with unprecedented spatial and time resolution (where the cooling and heating functions include photoionization and Compton effects, and restricting to models which include only radiative or only mechanical feedback in the form of nuclear winds), the effects of radiative and mechanical feedback on the gas flows in isolated elliptical galaxies. In particular, after having explored a few purely radiative feedback models, we explored two sequences of models in which the feedback is purely mechanical, and the only radiative effects allowed in the simulations are those due to gas cooling. The first sequence (Type A models) has a fixed mechanical efficiency as in most prior investigations, and the second (Type B models) allows the efficiency to increase with increasing accretion rate as indicated by the radiatively driven outflow models. It is difficult to know, either from fundamental physics calculations or from existing observations, what values of the mechanical energy efficiency to adopt, so we have tried a range of values from 5×10^{-3} to 10^{-5} to see which, if any, provides acceptable results, consistent with what is known about the properties of elliptical galaxies.

The investigation is in line with that of our previous papers, and the general framework is maintained. However, the galaxy models and some of the relevant input physics have been substantially improved and extended (see Table 1). As before, the recycled gas, arising from the evolving stars in the inner several kiloparsecs of the galaxy (assumed a giant elliptical), necessarily drives a classical radiative instability and a collapse toward the center of metal-rich gas. As a consequence, a starburst occurs and the central SMBH is fed. We confirm that steady accretion on SMBHs is only possible at very low Eddington ratios, and consistently with the work of other authors we note that independent of whether the feedback is mechanical or radiative no steady flow appears to be possible for Eddington ratios above $\simeq$0.01, and that whenever the luminosity is significantly above this limit both the accretion and the output luminosity are in burst mode. The details of how much gas is accreted on the central SMBH versus consumed in stars versus ejected from the center by energy input from the starburst and AGN are one of the main outcomes of these models. Relevant quantitative properties of the models are presented in Table 2, while the general results can be summarized as follows.

1. Radiative heating and radiation pressure on the ISM by photons emitted by the central AGN and by the starburst, without any mechanical input, greatly reduces the "cooling-flow catastrophe" problem, but leads to results that are still defective as compared with detailed observations of local elliptical galaxies, in that the central SMBH would be too bright and too massive, and the galaxy would be too blue, due to repeated bursts of central star formation.
2. Adding mechanical energy from an AGN wind with fixed efficiency can address the problems posed by pure cooling flows but does not give a solution that in detail satisfies the observations. If the chosen efficiency is large, then a giant burst and an explosive degassing of the galaxy occurs (consistent with the results of Di Matteo et al. 2005; Johansson et al. 2008, and other investigators). Only a small growth of the black hole occurs before the gas content of the galaxy drops to levels below what is observed in real elliptical galaxies and the systems at redshift $z = 0$ are computed to have thermal bremstrahlung X-ray luminosities orders of magnitude lower than those typically seen in nearby ellipticals. Finally, we do not get any late time AGN, and the duty cycle approaches unity. By contrast, very low values of the assumed efficiency do not prevent the cooling flows from causing more late time star formation (blue stellar cores) than is seen in most nearby ellipticals. It appears that there is no range of intermediate efficiencies that allows one to escape from both of these defects.
3. Models with mechanical energy efficiency proportional to the luminosity, as indicated both by observations and detailed two-dimensional hydrodynamical simulations for radiatively driven winds, perform better, but are still inadequate. We thus conclude that mechanical energy input of the type adopted here—by itself—is unable to provide appropriate levels of feedback that would leave ellipticals at the current epoch with the properties that they are observed to have. In fact, we find clear evidence that two additional

different forms of feedback are needed. The first, taking place during the high-luminosity phases, it is in the form of radiative feedback, and is required to limit the growth of the central SMBH. The other form of missing feedback is required during the quiescent, low-luminosity accretion phases (in particular at late epochs), as revealed by accretion luminosity values that, although very sub-Eddington, are still larger than observed. Of course, standard radiative feedback is not effective during such phases, and presumably the further reduction is provided by nuclear jets and/or thermally driven winds. We remark again that these results are based on one-dimensional simulations. It would be very important to have similar two-dimensional or three-dimensional simulations, with the same input physics, for a verification of the conclusions reported above, in particular when considering the issues related to strongly aspherical phenomena (such as the effective coupling of jets and nuclear winds with the ambient ISM), or the effect of the ISM angular momentum on the accretion rate.

4. We stress that in our study the initial conditions represent a galaxy with a central SMBH closely following the Magorrian relation, and with a stellar population already formed: such a system would be called a "dead and red" galaxy, without much evolution expected. However, one of the general consequences of our exploration is the fact that the recycled gas from dying stars is a major source of fuel for the central SMBH, and this can induce substantial QSO activity, even in the absence of external phenomena such as galaxy merging, and the simulations reveal how complex the evolution of an isolated galaxy, subject to internal evolution only, can be. We note that recently similar conclusions have been reached, by using different considerations, also by other authors (e.g., see Pierce et al. 2007; Li et al. 2008; Kauffmann & Heckman 2008).

Summarizing, neither models with purely radiative feedback nor those with mechanical feedback as adopted here alone seem to be able to match all of the basic observations of elliptical galaxies (see also Sijacki et al. 2008). Models with purely radiative feedback are unable, for any reasonable radiative efficiency, to forestall sufficiently the collapse of gas onto the central black hole. While they do reduce the mass far below what it would have been in the no feedback ("cooling flow") case, they do not reproduce the observed Magorrian relation and leave the central black hole with masses greater than $10^9\,M_\odot$, perhaps a factor of 4 too large. The models with purely mechanical feedback can, however, for an appropriate choice of the mechanical efficiency, match the well-established $M_{\rm BH}$–σ relation, but only for efficiencies chosen to be so large as to leave the galaxies with much less gas than is actually seen in normal ellipticals as determined by their X-ray luminosities. A more detailed discussion of other aspects of the difficulties encountered by the models with solely mechanical feedback, the description of the most successful combined models (which utilize both radiative and mechanical feedback), and their observational properties, is kept for the following papers (Papers II–V).

We thank Jenny Green, Jeremy Goodman, Silvia Pellegrini, Eve Ostriker, and Jim Stone for useful discussions, and Annibale D'Ercole and Dennis McRitchie for helpful suggestions on coding issues. We also thank the anonymous referee for careful reading and for comments that improved the presentation of the paper. D.P. acknowledges support by the National Aeronautics and Space Administration under Grant/Cooperative Agreement No. NNX08AE57A issued by the Nevada NASA EPSCoR program.

APPENDIX

A PHYSICAL BASIS FOR THE PHENOMENOLOGICAL MECHANICAL FEEDBACK EQUATION: INPUT FROM AGN WIND/JET TO HYDRODYNAMIC FLOW

In this Appendix, we describe the physics behind the phenomenological differential Equation (29) modeling the wind and jet mechanical interaction with the ISM of the galaxy: note that the treatment is formally identical for the jet and for the wind.

How can we estimate the rate of energy deposition from a conical wind or jet emitted by a central AGN into the ISM of the galaxy in which the SMBH is embedded? We will take from Sections 2.2 and 2.3 the estimates for the total outflowing mass rate in the wind or jet ($\dot{M}_{\rm dw}$ and $\dot{M}_{\rm j}$, Equations (17) and (19); we denote these quantities as $\dot{M}_{\rm wj}$), and the total mechanical energy flux ($L_{\rm dw}$ and $L_{\rm j}$, Equations (20) and (24); denoted as $L_{\rm wj}$). The solid angle of each cone, that we call in general $\Delta\Omega_{\rm c}$ (constant for the jet, and given by Equation (31) for the wind), has a *linear* opening angle $\Theta_{\rm c}$, so that $\Delta\Omega_{\rm c} = \pi\Theta_{\rm c}^2$. From elementary geometrical considerations, one obtains for the linear opening of the cone the relation $R_{\rm c}(r) = r\Theta_{\rm c}(r)$, $\dot{M}_{\rm wj} = v_{\rm wj}(r)\pi R_{\rm c}^2(r)\rho_{\rm wj}(r)$, and $L_{\rm wj} = 0.5\dot{M}_{\rm wj}v_{\rm wj}^2(r)$. As described in Section 2.3, the jets were taken to be very narrow and nearly relativistic, with energy efficiency increasing as $\dot{M}_{\rm BH}$ decreases. The winds were taken to have much larger opening angles, much lower (but still supervirial) velocities and to have an energy efficiency that increased with increasing $\dot{M}_{\rm BH}(t)$ (see Figure 1 for details).

Certainly, the simplest description that one could propose would be to imagine that no energy or mass was transferred from the outflowing supersonic flow to the ambient fluid until the internal momentum flux per unit area (declining as r^{-2}) reached the level where it locally matched the pressure in the ambient fluid, and define that radius ($R_{\rm wj}$) to be that of the working surface where the wind or jet dumped all of its mass, momentum, and energy. In this simplest of all models there would be no input from the wind or jet until this point was reached as the jet/wind was driven losslessly through the ISM of the galaxy. So, below the working surface, where $\beta(r) \equiv P_{\rm ISM}/P_{\rm wj} < 1$, the flow is conservative, but then as the pressure ratio approaches unity the mass and energy are deposited rapidly into a thin shell. While this approach has the virtue of simplicity and conservation of the vital quantities (and it was the first that we explored numerically), it is numerically unattractive and unstable.

Next, one could adopt the similar but smoother scheme described in Equation (29) but without the time-dependent term. In this case there are some losses below and above the working surface, but the bulk of the mass and energy are dumped into the ambient medium over approximately one scale length in radius in the vicinity of $R_{\rm wj}$. This is the equation that we adopted in this paper for adding energy and mass from the wind/jet to the ambient flow. This approach has assumed implicitly that all wind/jet outflow velocities are highly supersonic so that the quantities in the outflow at distance r from the center and at time t are essentially the same as at R_1 and t.

But it is straightforward to allow for propagation effects the finite time it takes for the wind/jet to flow from the first active grid point R_1 to r. Since the total mass, momentum, and

energy flux (integrated over the sphere) are conserved beyond R_1 aside from losses calculated explicitly (sinks, indicated in the following with S), we can write the more general equation

$$\frac{\partial Y}{\partial t} + v_{\rm wj}\frac{\partial Y}{\partial r} = -S(r,t). \quad \text{(A1)}$$

We then finally choose to write the sink term as $S(r,t) = Y/\tau(r,t)$, so that $dt/\tau(r,t)$ is the fraction of the outflow mass (or energy or momentum) flux that is deposited in time dt at (r,t). Consistent with the concept of depositing the mass, momentum, and energy smoothly in the vicinity of the working surface, we take

$$\frac{1}{\tau} = \frac{v_{\rm wj}}{r}\frac{P_{\rm ISM}}{P_{\rm wj}} = \frac{v_{\rm wj}}{r}\beta(r,t), \quad \text{(A2)}$$

where β is the pressure ratio. Inserting Equation (A2) in Equation (A1), and after some rearrangement, we obtain Equation (29). It reduces to our first, most simplified proposal (no explicit time-dependent term) in the limits that either the flow is steady or it is of very large velocity (i.e., $v_{\rm wj} \gg \max(v, c_{\rm s})$). The full Equation (29), which allows for the lags in a time-dependent flow, provides more stable solutions but is more costly to implement than the nontime-dependent form because the Courant condition for the time step must be modified to be

$$\Delta t < \min\left(\frac{\Delta r}{\sqrt{c_{\rm s}^2 + v^2}}, \frac{\Delta r}{v_{\rm wj}}\right), \quad \text{(A3)}$$

where Δr is the spatial grid spacing (for simplicity the contribution of artificial viscosity is not reported in equation above). In this paper, we used the more economical time-independent version rather than the more accurate but costly to implement full version, which is used and discussed in Paper III.

Now let us backup and ask if, for a steady conical flow, the time-independent equation can be derived by any more formal arguments drawn from first principles. For a steady conical flow, which interacts with the ambient flow only at its boundary, it is easy to derive the following equations from the conservation laws. If the linear opening angle of the cone is $\Theta_{\rm c}$, then from geometrical considerations

$$\frac{d\ln\Theta_{\rm c}}{d\ln r} = \frac{c_{\rm s}}{\Theta_{\rm c} v_{\rm wj}} - 1, \quad \text{(A4)}$$

where the velocity of each fluid element in the outflow perpendicular to the radial direction is assumed to be the speed of sound $c_{\rm s}$ in that flow at radius r. The equation of mass conservation is

$$\frac{d\ln\rho}{d\ln r} = -2 - \frac{d\ln v_{\rm wj}}{d\ln r} - 2\frac{d\ln\Theta_{\rm c}}{d\ln r}, \quad \text{(A5)}$$

and we are now allowing the flow velocity to be a function of radius. The first law of thermodynamics ($dU = dQ - PdV$) can be written as

$$2\frac{d\ln c_{\rm s}}{d\ln r} = (\gamma-1)\frac{d\ln\rho}{d\ln r} + \frac{\gamma-1}{c_{\rm s}^2}\frac{dq}{d\ln r}, \quad \text{(A6)}$$

where $q(r,t)$ is the heat energy added per unit mass of the flow. The conservation of energy (neglecting gravitational energy in this supervirial flow) can be written as

$$\frac{d\ln v_{\rm wj}}{d\ln r} = -\frac{2}{\gamma-1}\frac{c_{\rm s}^2}{v_{\rm wj}^2} + \beta(r)\frac{d\ln\rho}{d\ln r}, \quad \text{(A7)}$$

where we have allowed for the work done on the external fluid, as described below. We have not required that the pressure in the wind/jet balances the external pressure and in such a highly supersonic flow this would not naturally be the case (the jet fluid tending to rapidly cool due to the adiabatic expansion, i.e., $c_{\rm s}^2(r)\rho(r) \ll P_{\rm ISM}$). We can define the *equilibrium* internal speed sound, $c_{\rm eq}$, that would correspond to pressure equilibrium across the cone boundary as

$$\rho(r)c_{\rm eq}^2(r) \equiv P_{\rm ISM}(r), \quad \text{(A8)}$$

and in general we expect that, if $c_{\rm s}(r) \ll c_{\rm eq}(r)$, then the wind/jet will be unstable to rippling, internal shocks will develop, and we can plausibly assume that the heat generated by such processes will result in energy being taken from the bulk flow (reducing $v_{\rm wj}$) and being added to the thermal energy in the wind/jet, with the heat generated by the instability proportional to $c_{\rm eq}^2(r) - c_{\rm s}^2(r)$. Of course, additional phenomena such as strong shear and large density contrast at the wind/jet boundary are likely to give rise to instabilities there, regardless of the value of $c_{\rm s}$. Then, from dimensional analysis we would obtain

$$\frac{dq}{d\ln r} = \text{constant} \times \frac{c_{\rm eq}}{v_{\rm wj}} \times \left[c_{\rm eq}^2(r) - c_{\rm s}^2(r)\right]. \quad \text{(A9)}$$

Note that the instabilities converting forward kinetic energy in the wind/jet to thermal energy are also responsible for the source terms of mass, momentum, and energy transferred from the wind/jet to the ISM along the boundaries of the cone. The set of six Equations (A4)–(A9) would allow one to compute the radial dependence of the six variables ρ, $v_{\rm wj}$, $\Theta_{\rm c}$, $c_{\rm eq}$, $c_{\rm s}$, q (or in principle their more complicated time-dependent versions) to determine the rate at which energy and mass are drained from the sides of the wind/jet and from its working surface. If however the instabilities are very efficient, we can short circuit this process, drop the $q(r)$ variable and simply assume that heat is supplied to the outflow (and taken from the bulk motion) at the rate required to maintain $c_{\rm s}(r) = c_{\rm eq}(r)$. Then, omitting several steps of the straightforward algebra, and approximating the flow by power-law solutions (i.e., all variables are taken to scale as powers of the radius r), one obtains, in the case of a steady wind/jet

$$\frac{d\ln Y}{d\ln r} = -\beta(r)\left[\frac{2\gamma+\mu}{\gamma-1+\gamma\beta(r)}\right], \qquad \mu \equiv \frac{d\ln P_{\rm ISM}}{d\ln r}, \quad \text{(A10)}$$

which, aside from the bracket, is the same as the time-independent version of Equation (29) that we use in this paper. Typical values for the quantities in the brackets, considerably below the working surface are $\gamma = 5/3, \mu = -2, \beta \to 0$, so that the term in square brackets tends to the value of 2, giving a result which is very close to our time-independent version of Equation (29). The essential conclusion of this section is that, while a full two-dimensional or three-dimensional, time-dependent treatment of the energy and mss deposition from an outflowing wind/jet is highly desirable and in fact essential for a careful, quantitative treatment of this problem, nevertheless, the simple formulation presented in Equation (29) does offer a conservative scheme which captures several of the basic features of the problem.

REFERENCES

Antonuccio-Delogu, V., & Silk, J. 2008, MNRAS, 389, 1750
Arav, N., et al. 2007, ApJ, 658, 829

Begelman, M. C., & Nath, B. B. 2005, MNRAS, 361, 1387
Begelman, M. C., & Ruszkowski, M. 2005, Phil. Trans. R. Soc., 363, 655
Bertin, G., et al. 1994, A&A, 292, 381
Binney, J. 2001, in ASP Conf. Proc. 250, "Particles and Fields in Radio Galaxies Conference,", ed. R. A. Laing & K. M. Blundell (San Francisco, CA: ASP), 481
Binney, J., & Evans, N. W. 2001, MNRAS, 327, L27
Binney, J., & Tabor, G. 1995, MNRAS, 276, 663
Blustin, A. J., et al. 2007, A&A, 466, 107
Burkert, A., & Silk, J. 2001, ApJ, 554, L151
Cappellari, M., et al. 2006, MNRAS, 366, 1126
Castor, J. I., Abbott, D. C., & Klein, R. I. 1975, ApJ, 195, 157
Cavaliere, A., & Vittorini, V. 2002, ApJ, 570, 114
Chartas, G., Brandt, W. N., & Gallagher, S. C. 2003, ApJ, 595, 85
Churazov, E., Sazonov, S., Sunyaev, R., Forman, W., Jones, C., & Böhringer, H. 2005, MNRAS, 363, L91
Ciotti, L. 2009, Riv. Nuovo Cimento, 32, 1
Ciotti, L., Morganti, L., & de Zeeuw, P. T. 2008, MNRAS, 393, 491
Ciotti, L., & Ostriker, J. P. 1997, ApJ, 487, L105 (CO97)
Ciotti, L., & Ostriker, J. P. 2001, ApJ, 551, 131 (CO01)
Ciotti, L., & Ostriker, J. P. 2007, ApJ, 665, 1038 (CO07)
Cowie, L. L., Ostriker, J. P., & Stark, A. A. 1978, ApJ, 226, 1041
Crenshaw, D. M., Kraemer, S. B., & George, I. M. 2003, ARA&A, 41, 117
Croton, D. J., et al. 2006, MNRAS, 365, 11
Czoske, O., Barnabe', M., Koopmans, L. E. V., Treu, T., & Bolton, A. S. 2008, ApJ, 384, 987
de Zeeuw, P. T. 2001, in Proc. ESO Workshop 1999, ed. L. Kaper, E. P. J. van den Heuvel, & P. A. Woudt (Berlin: Springer), 78
Diehl, S., & Statler, T. S. 2008, ApJ, 687, 986
Di Matteo, T., Springel, V., & Hernquist, L. 2005, Nature, 433, 604
Dorodnitsyn, A., Kallman, T., & Proga, D. 2008, ApJ, 675, 5
Douglas, N. G., et al. 2007, ApJ, 664, 257
Dubinski, J., & Carlberg, R. G. 1991, ApJ, 378, 496
Dye, S., Evans, N. W., Belokurow, V., Warren, S. J., & Hewett, P. 2008, MNRAS, 388, 384
Faber, S. M., et al. 1997, AJ, 114, 1771
Fabian, A. C. 1999, MNRAS, 308, L39
Fabian, A. C., Thomas, P. A., Fall, S. M., & White, R. E., III. 1986, MNRAS, 221, 1049
Ferrarese, L., & Ford, H. 2005, Space Sci. Rev., 116, 523
Ferrarese, L., & Merritt, D. 2000, ApJ, 539, L9
Fukushige, T., & Makino, J. 1997, ApJ, 477, L9
Gallo, E., Treu, T., Jacob, J., Woo, J. H., Marshall, P., & Antonucci, R. 2008, ApJ, 680, 154
Ganguly, R., & Brotherton, M. S. 2008, ApJ, 672, 102
Gavazzi, R., Treu, T., Rhodes, J. D., Koopmans, L. V. E., Bolton, A. S., Burles, S., Massey, R. J., & Moustakas, L. A. 2007, ApJ, 667, 176
Gebhardt, K., et al. 2000, ApJ, 539, L13
Ghisellini, G. 2008, in Active Galactic Nuclei 8, ed. L. Lanteri, C. M. Raiteri, A. Capetti, & P. Rossi (Torino, Italy), http://agn8.oato.inaf.it
Goncalves, T. S., Steidel, C. C., & Pettini, M. 2008, ApJ, 676, 816
Graham, A. W., Erwin, P., Caon, N., & Trujillo, I. 2003, RevMexAA, 17, 196
Granato, G. L., De Zotti, G., Silva, L., Bressan, A., & Danese, L. 2004, ApJ, 600, 580
Haiman, Z., Ciotti, L., & Ostriker, J. P. 2004, ApJ, 606, 204
Hamann, F., Kaplan, K. F., Rodriguez Hidalgo, P., Prochaska, J. X., & Herbert-Fort, S. 2008, MNRAS, 391, L39
Helmboldt, J. F., Walterbos, R. A. M., & Goto, T. 2008, MNRAS, 387, 1537
Hernquist, L. 1990, ApJ, 356, 359
Ho, L. C. 2008, ARA&A, 46, 475
Holt, J., Tadhunter, C. N., & Morganti, R. 2008, MNRAS, 387, 639
Hopkins, P. F., Cox, T. J., Dutta, S. N., Hernquist, L., Kormendy, J., & Lauer, T. R. 2009a, ApJS, 181, 135
Hopkins, P. F., & Hernquist, L. 2008, arXiv:0809.3789
Hopkins, P. F., Hernquist, L., Cox, T. J., Robertson, B., Di Matteo, T., & Springel, V. 2006, ApJ, 639, 700
Hopkins, P. F., Lauer, T. R., Cox, T. J., Hernquist, L., & Kormendy, J. 2009b, ApJS, 181, 486
Humphrey, P. J., Buote, D. A., Gastaldello, F., Zappacosta, L., Bullock, J. S., Brighenti, F., & Mathews, W. G. 2006, ApJ, 646, 899
Jaffe, W. 1983, MNRAS, 202, 995
Jaffe, W., Ford, H. C., O'Connell, R. W., van den Bosch, F. C., & Ferrarese, L. 1994, AJ, 108, 1567
Jiang, Y.-F., Ciotti, L., Ostriker, J. P., & Spitkovsky, A. 2009, ApJ, submitted (arXiv:0904.4918)
Johansson, P. H., Naab, T., & Burkert, A. 2008, Astron. Nachr., 329, 956
Jolley, E., & Kuncic, Z. 2008, MNRAS, 386, 989
Kauffmann, G., & Heckman, T. M. 2008, arXiv:0812.1224
King, I. R. 1972, ApJ, 174, L123
King, A. R. 2003, ApJ, 596, L27
Kirkman, D., & Tytler, D. 2008, MNRAS, 391, 1457
Königl, A. 2006, Mem. Soc. Astron. Ital., 77, 598
Koopmans, L. V. E., Treu, T., Bolton, A. S., Burles, S., & Moustakas, L. A. 2006, ApJ, 649, 599
Kormendy, J., & Richstone, D. 1995, ARA&A, 33, 581
Kurosawa, R., & Proga, D. 2008, ApJ, 674, 97
Kurosawa, R., & Proga, D. 2009, ApJ, 693, 1929
Lauer, T. R., et al. 2005, AJ, 129, 2138
Li, C., Kauffmann, G., Heckman, T. M., White, S. D. M., & Jing, Y. P. 2008, MNRAS, 385, 1915
Magorrian, J., et al. 1998, AJ, 115, 2285
Marconi, A., & Hunt, L. K. 2003, ApJ, 589, L21
Martinez-Sansigre, A., & Taylor, A. M. 2009, ApJ, 692, 964
Martini, P. 2004, in Coevolution of Black Holes and Galaxies, ed. L. C. Ho (Cambridge: Cambridge Univ. Press), 169
McCarthy, I. G., Babul, A., Bower, R. G., & Balogh, M. L. 2008, MNRAS, 386, 1309
McLure, R. J., & Dunlop, J. S. 2002, MNRAS, 331, 795
McNamara, B. R., & Nulsen, P. E. J. 2007, ARA&A, 45, 117
Merloni, A., & Heinz, S. 2008, MNRAS, 388, 1011
Milosavljevic, M., Bromm, V., Couch, S. M., & Oh, S. P. 2008, arXiv:0809.2404
Morgan, C. W., Kochanek, C. S., Morgan, N. D., & Falco, E. M. 2007, arXiv:0707.0305
Murray, N., Quataert, E., & Thompson, T. A. 2005, ApJ, 618, 569
Narayan, R., & Yi, I. 1994, ApJ, 428, L13
Navarro, J. F., Frenk, C. S., & White, S. D. M. 1997, ApJ, 490, 493
Nayakshin, S., Dehnen, W., Cuadra, J., & Genzel, R. 2006, MNRAS, 366, 1410
Nayakshin, S., & Sunyaev, R. 2005, MNRAS, 364, L23
Noble, S. C., Krolik, J. H., & Hawley, J. F. 2009, ApJ, 692, 411
Omma, H., Binney, J., Bryan, G., & Slyz, A. 2004, MNRAS, 348, 1105
Ostriker, J. P., & Ciotti, L. 2005, Phil. Trans. R. Soc., 363, 667 (OC05)
O'Sullivan, E., Ponman, T. J., & Collins, R. S. 2003, MNRAS, 340, 1375
Parriott, J. R., & Bregman, J. N. 2008, ApJ, 681, 1215
Pellegrini, S. 2005a, ApJ, 624, 155
Pellegrini, S. 2005b, MNRAS, 364, 169
Pellegrini, S., & Ciotti, L. 1998, A&A, 333, 433
Pellegrini, S., Ciotti, L., & Ostriker, J. P. 2009, Adv. Space Res., in press (arXiv:0904.3421)
Peterson, J. R., & Fabian, A. C. 2006, Phys. Rep., 427, 1
Pierce, C. M., et al. 2007, ApJ, 660, L19
Pipino, A., Kaviraj, S., Bildfell, C., Hoekstra, H., Babul, A., & Silk, J. 2009b, MNRAS, 395, 462
Pipino, A., Silk, J., & Matteucci, F. 2009a, MNRAS, 392, 475
Prochaska, J. X., & Hennawi, J. F. 2009, ApJ, 690, 1558
Proga, D. 1999, MNRAS, 304, 938
Proga, D. 2007a, ApJ, 661, 693
Proga, D. 2007b, in ASP Conf. Ser. 373, The Central Engine of Active Galactic Nuclei, ed. L. C. Ho & J. M. Wang (San Francisco, CA: ASP), 267
Proga, D., & Kallman, T. 2002, ApJ, 565, 455
Proga, D., & Kallman, T. 2004, ApJ, 616, 688
Proga, D., Ostriker, J. P., & Kurosawa, R. 2008, ApJ, 676, 101
Proga, D., Stone, J. M., & Drew, J. E. 1998, MNRAS, 295, 595
Proga, D., Stone, J. M., & Kallman, T. 2000, ApJ, 543, 686
Rafferty, D. A., McNamara, B. R., & Nulsen, P. E. J. 2008, ApJ, 687, 899
Renzini, A., Ciotti, L., D'Ercole, A., & Pellegrini, S. 1993, ApJ, 419, 52
Riciputi, A., Lanzoni, B., Bonoli, S., & Ciotti, L. 2005, A&A, 443, 133
Rusin, D., & Kochanek, C. S. 2005, ApJ, 623, 666
Rusin, D., Kochanek, C. S., & Keeton, C. R. 2003, ApJ, 595, 29
Saglia, R. P., et al. 1993, A&A, 403, 567
Sazonov, S. Yu., Krivonos, R., Revnivtsev, M., Churazov, E., & Sunyaev, R. A. 2008, A&A, 482, 517
Sazonov, S. Yu., Ostriker, J. P., Ciotti, L., & Sunyaev, R. A. 2005, MNRAS, 358, 168
Sazonov, S. Yu., Ostriker, J. P., & Sunyaev, R. 2004, MNRAS, 347, 144
Sazonov, S. Yu., Revnivtsev, M., Krivonos, R., Churazov, E., & Sunyaev, R. A. 2007, A&A, 462, 57
Schawinski, K., et al. 2009, ApJ, 690, 1672
Shakura, N. I., & Sunyaev, R. A. 1973, A&A, 24, 337
Shi, J., & Krolik, J. 2008, ApJ, 679, 1018
Sijacki, D., Pfrommer, C., Springel, V., & Ensslin, T. A. 2008, MNRAS, 387, 1403
Sijacki, D., Springel, V., Di Matteo, T., & Hernquist, L. 2007, MNRAS, 380, 877

Silk, J., & Rees, M. J. 1998, A&A, 331, L1
Soltan, A. 1982, MNRAS, 200, 115
Somerville, R. S. 2008, in ASP Conf. Ser. 399, Panoramic Views of Galaxy Formation and Evolution, ed. T. Kodama, T. Yamada, & K. Aoki (San Francisco, CA: ASP), 391
Springel, V., Di Matteo, T., & Hernquist, L. 2005, MNRAS, 361, 776
Tabor, G., & Binney, J. 1993, MNRAS, 263, 323
Trager, S. C., Faber, S. M., & Dressler, A. 2008, MNRAS, 386, 715
Treu, T., & Koopmans, L. V. E. 2002, ApJ, 575, 87
Treu, T., & Koopmans, L. V. E. 2004, ApJ, 611, 739
Turnshek, D. A. 1988, in QSO Absorption Lines: Probing the Universe, ed. J. C. Blades, D. A. Turnshek, & C. A. Norman (Cambridge: Cambridge Univ. Press), 17
Vernaleo, J. C., & Reynolds, C. S. 2006, ApJ, 645, 83
Voit, G. M., & Donahue, M. 2005, ApJ, 634, 955
Wang, J. M. 2008, ApJ, 682, L81
Watabe, Y., Kawakatu, N., & Imanishi, M. 2008, ApJ, 677, 895
Woo, J. H., Treu, T., Malkan, M. A., & Blandford, R. D. 2008, ApJ, 681, 925
Wrobel, J. M., Terashima, Y., & Ho, L. C. 2008, ApJ, 675, 1041
Wyithe, J. S. B., & Loeb, A. 2003, ApJ, 595, 614
Yu, Q., & Tremaine, S. 2002, MNRAS, 335, 965